Department of Energy
Carlsbad Field Office
P. O. Box 3090
Carlsbad, New Mexico 88221

April 21, 2025

Mr. Tom Peake, Director
Center for Waste Management and Regulations
William Jefferson Clinton Building, West
1301 Constitution Ave NW, Mail Code 6608T
Washington, D.C. 20004

Subject: Response 8 to U.S. Environmental Protection Agency's Questions on the Replacement Panels Planned Change Request

Reference: EPA letter from Tom Peake to Michael Gerle, dated September 5, 2024; Subject: Sixth Set of questions on the Replacement Panels Planned Change Request

Dear Mr. Peake:

Enclosed is the U.S. Department of Energy (DOE) response to the U.S. Environmental Protection Agency's (EPA) questions on the Replacement Panels Planned Change Request (RPPCR) received in the above reference letter. In this communication, the DOE is responding to twenty of the EPA's questions. This submittal includes two enclosures:

- Enclosure 1 provides the DOE's responses to twenty of the EPA's technical questions and comments on the RPPCR.
- Enclosure 2 is a status report of the DOE's responses to the EPA questions on the RPPCR. The report shows the status of all EPA technical questions and comments received to date.

The DOE will continue to submit phased responses to the EPA to ensure questions are answered as promptly as possible. Below is one of the responses provided in Enclosure 1.

EPA Letter Date	EPA Question Number	EPA Question Description
September 5, 2024	RPPCR6-Bhperm-1 through 20	Information requests for DOE related to the selection of a new upper bound on the permeability of a degraded borehole.

CBFO:ERCD:MG:RS:25-0278

If you have any questions, please contact Dr. Anderson Ward, Compliance Certification Manager, CBFO Environmental Regulatory Compliance Division. Dr. Ward can be reached at (575) 988-5414.

Sincerely,

MICHAEL GERLE

Digitally signed by MICHAEL GERLE
Date: 2025.04.21 14:06:56 -06'00'

Michael Gerle, Director
Environmental Regulatory
Compliance Division
Carlsbad Field Office

Enclosures (2)

cc: w/enclosures

M. Bollinger, CBFO	*ED
E. Garza, CBFO	ED
M. Hall, CBFO	ED
A. Ward, CBFO	ED
Z. Lepchitz, CBFO	ED
J. Adkins, CBFO	ED
R. Chavez, SIMCO	ED
R. Flynn, SIMCO	ED
M. Gonzales, SIMCO	ED
M. Jones, SIMCO	ED
R. Salness, SIMCO	ED
J. Settle, SIMCO	ED
S. Strong, SIMCO	ED
A. Waldram, SIMCO	ED
M. Cook, LATA	ED
K. Day, LATA	ED
S. Harper, LATA	ED
J. Haschets, LATA	ED
R. Hernandez, LATA	ED
M. Serrano, LATA	ED

*ED denotes electronic distribution

Enclosure 1

Department of Energy Response 8 to EPA's Questions on the RPPCR

Table of Contents

List of Figures

List of Tables

Topic 1: Requests related to Gjerapic et al. (2023, Section 2.1) on the hydraulic conductivity of degraded steel and the relevance and applicability of permeable reactive barrier (PRB) granules as a surrogate for degraded steel casing

The Agency recognizes that direct measurements of the permeability of corroded iron are uncommon but concludes that the arguments put forth by Gjerapic et al. (2023) do not adequately demonstrate 1) that corroded PRB granules are reasonable surrogates for corroded borehole casing; 2) that the PRB column tests of Moraci et al. (2016) adequately simulate borehole conditions at WIPP; 3) that the proposed maximum corrosion product permeability of 10^{-15} m^2 is actually bounding; and 4) that the test results are consistent with the Thompson conceptual model for changes in borehole degradation processes with depth. It is also not clear how Gjerapic et al. intend to use the permeability information from PRB granules.

RPPCR6-Bhperm-1: PRB granules as surrogates for corroded borehole casing

Please provide justification that includes relevant experiments, data, and literature citations for the assumption that corroded PRB granules are reasonable surrogates for corroded borehole casing.

DOE Response

Corroded PRB granules are not a "reasonable surrogate" for corroded steel casing. Rather, the hydraulic conductivity (*K*) of intact PRB is selected as a conservative upper bound for degraded steel casing in unconfined conditions. The *K* of intact PRB is the highest for a manufactured iron-based material reported in the literature. It is reasonable to expect that a random assembly of corroded steel particles (e.g., resulting from pitting and degradation) would have a lower *K* than intact PRB. Hydraulic conductivity values in this document typically refer to the flow of fresh water at 25°C with the unit weight of $\gamma_w = 9.8\ kN/m^3$ and the dynamic viscosity of $\mu_w \approx 10^{-3} Pa \cdot s$ to facilitate easier comparison with existing literature data. Consequently, the reported hydraulic conductivity (*K*) values and the corresponding permeability (*k*) values are used interchangeably throughout this document, assuming the following relationship (see, e.g., Bear 1972, Equation 5.5.1)

$$K = \frac{\gamma_w k}{\mu_w} \quad (1)$$

Particles of corroded steel in a borehole, represented as viscoelastic porous media, undergo creep deformations and associated borehole pressures, which can be expected to reduce hydraulic conductivity over time. The borehole hydraulic conductivity is expected to decrease with the corresponding decrease in pore sizes (increase in specific surface area) and the increase in solid fraction (see, e.g., Torquato 2002, Section 16, Equation 16.99, and Section 18, Figure 18.11). If one considers potential porous configurations within the intrusion borehole, the polydisperse solids within the borehole are likely to form complex flow paths, which could significantly reduce the initial borehole permeability. In other words, the degraded borehole permeability is expected to be significantly lower than the permeability of the PRB. Unlike the monodisperse PRB matrix, the particle size distribution of borehole materials is not expected to be uniform and is likely to exhibit continuous permeability reduction, as small particles may occupy pores formed between larger particles, thereby reducing porosity (see, e.g., Bear 1972, Section 2.5.2). These "small" particles may be introduced by brine precipitation, steel and

cement degradation, and mechanical crushing of particles within the porous matrix due to increased confining pressures (creep) and volume expansion caused by steel corrosion. Therefore, the PRB hydraulic conductivity was used as a conservative estimate for the upper bound permeability of the degraded borehole fill materials assuming zero or very low confinement. Notably, the permeability of intact/uncorroded PRB (10^{-10} m^2) is an order of magnitude higher than that of the degraded borehole fill used in current performance assessment (PA) calculations (see, e.g., DOE 2019, Appendix PA-2019, Table PA-26).

RPPCR6-Bhperm-2: discrepancy in upper bound permeability for degraded steel casing

Please clarify the following discrepancy. The concluding paragraph on p. 7 for Section 2.1 of Gjerapic et al. (2023) identifies 10^{-15} m^2 as an upper bound permeability for degraded steel casing, but on p. 13 of Section 3.1, 10^{-10} m^2 is identified as the upper bound. EPA understands that the objective of the Gjerapic et al. analysis is to identify a single upper bound value and finds these statements to be contradictory.

DOE Response

The upper bound permeability of 10^{-15} m^2 is assumed for parts of the borehole consisting of degraded steel casing after long-term exposure to the corrosive Waste Isolation Pilot Plant (WIPP) environment, such as brines from the Salado and Castile formations. These borehole parts are subjected to long-term creep pressures and deformations of the surrounding Salado Formation and contain occluded air bubbles and precipitates within the porous matrix, analogous to the reported performance of iron-based materials in corrosive environments by Moraci et al. (2016).

In contrast, the initial upper bound (maximum) permeability of 10^{-10} m^2 was assigned to parts of the borehole that contain degraded steel. These parts have not yet experienced increased confining loads from the creep of the surrounding Salado Formation or long-term changes in permeability ("plugging effects") due to salt precipitation and gas exsolution. Hence, the maximum permeability of 10^{-10} m^2 for corroded steel was used to initiate creep calculations. These calculations assumed that the initial state of the previously open borehole, representing its undeformed configuration at time zero, now contains loose steel particles. The 10^{-10} m^2 is the maximum reported permeability for the manufactured iron-based material used in engineering practice (e.g., Permeable Reactive Barriers). The initial permeability of 10^{-10} m^2 is one order of magnitude smaller than the 10^{-9} m^2 assigned to an open borehole in PA calculations.

RPPCR6-Bhperm-3: PRB column test conditions

Please explain the conditions under which the PRB column tests of Moraci et al. (2016) were performed and how well those tests adequately simulate borehole conditions at WIPP.

DOE Response

Moraci et al. (2016) performed permeability tests in 5-cm diameter x 50-cm high plexiglass columns. The columns were filled with granular iron (D_{50}≈0.5mm) and had a mean porosity (ϕ) of 47 percent. The remaining void space was filled with washed quartz gravel. The columns of granular iron (PRB material) were subjected to upward flow at rates of 0.1, 0.5, and 2.5 ml/min. The influent contained dissolved metals, as summarized in Table 1.

Table 1. Moraci et al. (2016) test conditions

Test ID	Contaminant	Concentration (mg/L)	PRB Mass (g)	Thickness (cm)
A	Ni	40	1680	22.5
B	Ni	40	1680	22.5
C	Ni	50	240	3
D	Ni	8	240	3
E	Ni, Cu, Zn	50, 500, 50	240	3
F	Ni	8	1680	22.5
G	Ni	95	1680	22.5

The metallic species (contaminants) in Table 1 were introduced into the solution by dissolving nickel (II) nitrate hexahydrite, copper (II) nitrate hydrate, and zinc (II) nitrate hexahydrate. The concentrations of metallic species are lower than those of dissolved species and suspended solids, as reported by Popielak et al. (1983). Specifically, Popielak et al. (1983) report that the concentration of suspended solids varies from 45 mg/L at WIPP-12 to 87 mg/L at ERDA-6 (see Table C.2 in Popielak et al. 1983). Therefore, the permeability reduction ("plugging" potential) associated with the generation of precipitates in the WIPP environment is expected to be significantly higher than reported in Moraci et al. (2016) experiments.

While Moraci et al. (2016) experimental conditions are different from the WIPP conditions (e.g., the rate of corrosion is likely to be significantly higher at WIPP due to the presence of sulfates and chlorides in WIPP brines), the Moraci et al. (2016) results provide a guide that may be used to qualitatively explain the behavior observed during well testing at WIPP and predict the long-term hydraulic conductivity of borehole materials. Moraci et al. (2016) noted that the permeability of the PRB material decreased up to approximately five orders of magnitude with time due to:

1. the constriction of effective flow diameter due to iron corrosion and the associated volume expansion;

2. contaminant precipitation, leading to a reduction in the porosity and restricted flow; and

3. the entrapment of gas bubbles (e.g., hydrogen) generated during corrosion within the PRB matrix, resulting in a restriction to flow.

During WIPP well testing in ERDA-6 and WIPP-12, Popielak et al. (1983) reported flow restrictions, testing delays due to salt precipitation within the flow lines, gas exsolution from brine, and corrosion of flow meters. Both wells indicated a significant gas exsolution potential and higher corrosion potential than Moraci et al. (2016) reported. Consequently, there is a greater potential for a reduction in borehole permeability due to plugging of the porous matrix in the WIPP environment than Moraci et al. (2016) reported.

RPPCR6-Bhperm-4: scatter and uncertainty in experimental results of Moraci et al. (2016)

The experimental results of Moraci et al. (2016) on PRB permeability shown in Gjerapic et al. (2023, Figure 2) illustrate scatter and uncertainty that do not appear to have been taken into account in identifying $10^{-15} m^2$ as a bounding permeability. Please discuss and evaluate the impact of this uncertainty on the proposed bounding permeability of $10^{-15} m^2$

DOE Response

The proposed upper bounding borehole permeability refers to the "effective" permeability, k_{eff}, of the borehole. The k_{eff} represents the inverse of the flow resistance of individual borehole components, such as cement grout, steel casing, and the surrounding rock mass. It considers the resistance to flow along the interfaces between these components. In this context, low resistance to flow corresponds to high k_{eff} values. While the permeability of individual components is important for parameterizing the flow equation for the borehole, the *in-situ* permeability measurements and the overall borehole performance are always evaluated in terms of "effective" permeabilities.

Experimental results by Moraci et al. (2016) were taken as a qualitative estimate of the potential permeability reduction due to the loss of available flow space within the porous matrix of degraded steel caused by corrosion and the presence of gas and mineral precipitation. The proposed bounding borehole permeability estimates of 10^{-14} m^2 and 10^{-15} m^2 were based on the totality of the available information and account for:

- expected borehole/cement plug degradation rates (see, e.g., Matteo and Scherer 2012);
- relevant research and engineering standards on steel corrosion in aggressive environments (see, e.g., Subramanian 2008; NPL 2020; ISO 9223);
- reported rates of degradation for cement plugs considering WIPP-specific conditions (Bonen 1996) and permeability of cement plugs in aggressive environments (see, e.g., Curtice and Mallow 1979);
- reported field and laboratory measurements on borehole plugs (see, e.g., Christensen and Hunter 1980); and
- expected creep behavior (Reedlunn et al. 2022).

Aggressive environments, in terms of steel corrosion potential, were assumed to coincide with high levels of chloride ions, such as those encountered in maritime environments. Hence, maximum steel corrosion rates were estimated from literature sources that evaluated the corrosion impacts of aggressive species, including chlorides (e.g., Subramanian 2008). Similarly, aggressive environments for cement degradation considered hydraulic performance in the presence of brine and elevated temperatures. Considering the uncertainty in the long-term prediction of permeability in a borehole annulus, the upper bound permeability bound was established using the cement plug rather than corroded steel. Based on the available WIPP-specific performance data (see, e.g., Christensen and Hunter 1980) and relevant literature on the flow through porous media (see, e.g., Bear 1972, Section 5.8), the selected upper bound

values for borehole permeability, 10^{-14} m^2 and 10^{-15} m^2, are considered to have a very low (statistically negligible) exceedance probability. For example, the effective permeability of a 30-m-long cement plug will be governed by the least permeable section along the vertical flow path. Therefore, the permeability measurements obtained on shorter plugs (including measurements that allow for leakage through the tubing packer assembly), such as measurements presented in Table 2, are expected to provide an upper bound estimate for the effective permeability of a 30-m plug. For the average effective permeability of 1.6×10^{-16} m^2 (based on the geometric mean of permeability values in Table 2), the mean permeability of a cement plug is expected to range from 3.0×10^{-17} to 8.1×10^{-16} m^2 with the confidence level of 95 percent, and from 1.0×10^{-17} to 2.4×10^{-15} m^2 with the confidence level of 99 percent. These estimates were determined by applying Student's t-distribution to the logarithm of permeability values in Table 2, i.e., using permeability measurements for short "leaky" plugs. Considering the design length of the plug (30 meters) and the long-term effects of creep, there is high confidence that the upper bound for the borehole permeability remains below 10^{-14} m^2 for the plugs installed above the repository and below 10^{-15} m^2 for the plugs installed below the repository.

Gjerapic et al. (2023) note that the upper bound permeability of corroded steel casing, representing a fraction of the porous matrix with the effective permeability, k_{eff}, should focus on the "degraded steel permeability in areas subjected to significant confining pressures." This is particularly relevant in areas where cement plugs have been installed. The upper bound borehole permeabilities have been determined to be 10^{-14} m^2 for the upper borehole (above the repository) and 10^{-15} m^2 for the lower borehole (below the repository). These values were selected based on the maximum reported permeability results from experiments conducted under WIPP-specific conditions (see, e.g., Christensen and Hunter [1980] and the data in Table 2). In addition, these values consider literature-reported conditions that are likely to represent less favorable environments (see, e.g., Curtice and Mallow 1979), i.e., environments with higher effective permeabilities than expected at the WIPP site. Curtice and Mallow (1979) suggest that their experimental conditions are likely to result in faster steel/cement degradation of cement plugs than expected in the WIPP environment due to the increased interface flow potential. Experimental results by Stormont et al. (2018) and Curtice and Mallow (1979) include permeability tests conducted on relatively short samples with a steel casing, which support the selection of upper-bound borehole permeability values of 10^{-14} m^2 and 10^{-15} m^2.

The upper bound permeability of steel casing is established by considering data reported by Moraci et al. (2016) and Thompson et al. (1996). Thompson et al. (1996) noted that although corrosion products are exceptionally fine-grained, corrosion mechanics would likely generate debris with textures ranging from coarse to very fine. However, Thompson et al. (1996) neglected the effects of gas exsolution and mineral precipitation (e.g., Section B.5.3), which can reduce porosity and cause plugging, as observed by Moraci et al. (2016). Thompson et al. (1996) also assumed that radial diffusion was the principal mechanism leading to complete plug degradation. It was also argued that although it was inconceivable that dissolution and corrosion could combine to create a significant vertical pathway for flow, the capacities were more than enough to create horizontal pathways into the casing (Thompson et al. 1996). However, in this work, the effects of radial plug degradation are dismissed as a viable physical and chemical mechanism. This is due to the predicted confining pressures (see, e.g., Reedlunn et al. 2022), plug degradation mechanisms (Onofrei et al. 1992; Matteo and Scherer 2012), site-specific data (Bonen 1996), and industry practices (Cowie 2009; NPL 2020).

For granular iron-based PRB systems with high initial permeabilities, the long-term permeability value has been known to decrease over time, as demonstrated by laboratory experiments (see, e.g., Moraci et al. 2016) and field studies (see, e.g., Johnson and Tratnyek 2008). For example, Johnson and Tratnyek (2008) discuss the PRB performance installed at the Cornhusker Army Ammunition Plant (CAAP) near Grand Island, Nebraska. Johnson and Tratnyek (2009) report that the "plugged" CAAP PRB permeability was approximately 4×10^{-13} m² within a couple of years of installation. The PRB installed at CAAP was constructed using a mixture of iron and sand (30% by weight iron) and features a relatively large cross-sectional area ($A_{CAAP} \approx 79$ m^2) in comparison to the WIPP borehole ($A_{bh} \approx 0.08$ m^2). In addition, the CAAP PRB is subjected to a relatively low confining stress of about 0.2 MPa or less, while the cement plugs in the WIPP borehole will be subjected to a confining stress of 5 MPa or more. Furthermore, the groundwater chemistry at the CAAP site is expected to result in lower corrosion rates and reduced plugging potential compared to the WIPP brines. Hence, even without considering the effects of creep, the confining stress magnitude, and the presence of cement plugs, a reasonable long-term upper bound estimate for the borehole permeability may be set between 10^{-13} and 10^{-14} m^2.

As noted by Subramanian (2008), "Corrosion of steel exposed to concrete/grout occurs by a complex mechanism through metal dissolution at the concrete/metal interface". Therefore, the upper bound borehole permeability estimates must consider the degradation potential for steel and cement materials in the intrusion borehole. For a more realistic assessment of the upper bound borehole permeability, the presence of cement plugs and WIPP-specific data reported by Christensen and Hunter (1980) were taken into account.

Christensen and Hunter (1980) reported permeabilities for a 1.8-meter-long cement plug ranging from 0.03 to 0.6 millidarcy (mD) or 2.7×10^{-17} to 6.0×10^{-16} m^2, as shown in Table 2.

Table 2. Permeability of a 1.8-meter-long cement plug, after Christensen and Hunter (1980)

Test No.	Date	Permeability (mD)	Permeability (m^2)
1	10/9/1979	0.027	2.7E-17
2	10/10/1979	0.057	5.6E-17
3	10/19/1979	0.385	3.8E-16
4	12/12/1979	0.607	6.0E-16
5	12/21/1979	0.275	2.7E-16

Assuming a log-normal permeability distribution, the 95-percentile permeability range is between 1.8×10^{-17} and 1.4×10^{-15} m^2 with a mean of 1.6×10^{-16} m^2. At the 99.9% confidence level, the estimated mean permeability lies between 2.5×10^{-17} and 9.8×10^{-16} m^2.

For a random distribution of permeabilities along the length of the plug, the "effective" permeability is dominated by sections with lower values. For example, consider a cement plug consisting of N sections with a piece-wise constant permeability. The "effective" permeability, $k_{eff,plug}$, of such a plug can be determined as (see, e.g., Bear 1972, Section 5.8.1):

$$k_{eff,plug} = \frac{L_{eff,plug}}{\sum_{i=1}^{N} \frac{L_i}{k_i}} \quad (2)$$

where L_i is the length of the i[th] section, k_i is the permeabilities of the i[th] section, and $L_{eff,plug}$ is the length of the plug. For a 9-m-long plug with five 1.8-m sections and the permeabilities in Table 2, the effective permeability is:

$$\mathrm{k_{eff,plug}} = \frac{9}{\frac{1.8}{0.027}+\frac{1.8}{0.057}+\frac{1.8}{0.385}+\frac{1.8}{0.607}+\frac{1.8}{0.275}} = 0.080\ \mathrm{md}\ (7.9 \times 10^{-17}\mathrm{m}^2) \quad (3)$$

The resulting $k_{eff,plug}$ of 7.9×10^{-17} m^2 (0.08 mD) is lower than the geometric mean permeability of 1.6×10^{-16} m^2. Therefore, the $k_{eff,plug}$ of the cement plug, which includes the cement grout and the surrounding corroded steel casing, is dominated by sections of the plug with smaller permeabilities.

The above arguments can be extended to determine the upper bound of the effective borehole permeability, k_{eff}, used in PA calculations. Notably, k_{eff} is dominated by sections with lower k_i (e.g., cement plug locations) rather than locations with lower resistance to flow (e.g., voids remaining after plug installation).

For WIPP scenarios, assuming low corrosion rates and early closure times, it is reasonable to assume the presence of relatively loose material within open sections of the borehole. These sections may be modeled by assuming permeabilities between 10^{-9} and 10^{-10} m^2. These permeabilities assume that flow occurs without significant restrictions or through degraded materials with a permeability corresponding to that of the intact PRB material (e.g., the highest k in Figure 2 of Gjerapic et al. 2023). At longer times in more corrosive environments, the k_{eff} of the open borehole may reach 10^{-15} m^2, which is consistent with the reduced permeability at large times reported in Figure 12 of Moraci et al. (2016). Assuming a cement plug $k_{eff,plug} = k_{plug}$ of 10^{-17} m^2 at early time under low corrosion rates and 6.0×10^{-16} m^2 for high corrosion rates, the upper bound permeability k_{eff} is estimated as follows:

$$k_{eff} = \frac{L_{open}+L_{plug}}{L_{open}/k_{open}+L_{plug}/k_{plug}} \quad (4)$$

where

k_{eff} = effective permeability of the borehole consisting of two parts/sections: the (initially) open annulus and the cement plug (m^2)
L_{open} = length of the borehole section with the (initially) open annulus (m)
L_{plug} = length of the cement plug (m)
k_{open} = permeability of the borehole section with the (initially) open annulus (m^2)
k_{plug}= permeability of the cement plug (m)

Table 3 summarizes the upper bound k_{eff} for a borehole with an effective length $L_{eff} = L_{open} + L_{plug}$ extending from the bottom of the Rustler Formation to the waste repository level. These calculations assume an open section of 400 m and a plug length of 30 m.

Table 3. Upper bound k_{eff} for an open borehole based on PRB data from Moraci et al. (2016)

Environmental Condition	[1]k_{open} (m^2)	k_{plug} (m^2)	[2]k_{eff} (m^2)
Low corrosion rates and early times after closure[3]	1.00E-09	1.00E-17	1.43E-16
	1.00E-10	1.00E-17	1.43E-16
High corrosion rates[4,5]	1.00E-15	6.00E-16	9.58E-16
	1.00E-10	6.00E-16	9.21E-15

Notes:

1. Open borehole permeability refers to sections of the borehole with an open annulus immediately after installing the cement plugs.
2. "Effective" borehole permeability values were determined for the "upper borehole" (borehole section above the repository)
3. "Effective" permeability for low corrosion rates was determined for L_{open} =400 m and L_{plug} =30 m
4. "Effective" permeability for high corrosion rates was determined for L_{open} =402 m, L_{plug} =28 m
5. The long-term open borehole permeability of 10^{-10} m^2 is not physically possible if borehole materials are subjected to high corrosion rates and creep deformations of the surrounding rock mass.

RPPCR6-Bhperm-5: relevance of Moraci et al. column tests to WIPP conditions

The PRB permeability in the Moraci et al. (2016) experiments decreased by five orders of magnitude in one year, presumably due to corrosion. The corrosion rate in those experiments appears to far exceed the corrosion rates observed in Delaware Basin boreholes (see discussion in Section 5.2 and Appendix B.5.1 of Thompson et al. 1996). Please describe the physical characteristics of the PRB granules and experimental conditions under which the results of Moraci et al. (2016) column tests were obtained and explain why the results of Moraci et al.'s tests are relevant to the chemical and physical conditions associated with borehole casing corrosion at WIPP.

DOE Response

Moraci et al. (2016) conducted experiments using the PRB material consisting of granular iron (D_{50} ≈ 0.5 mm, ϕ = 47%). Moraci et al. (2016) attributed the observed loss in permeability values to several mechanisms (the corrosion mechanism is often not dominant):

1. constriction of effective flow diameter due to iron corrosion (iron volume expansion);
2. contaminant precipitation leading to a reduction in the porosity and restricted flow;
3. hydrogen bubbles generated during the corrosion process are entrapped within the PRB porous matrix, presenting restrictions to flow.

Based on the comparison between Moraci et al. (2016) and WIPP-specific data, the plugging mechanisms and corrosion rates will likely be more severe at the WIPP site. Moraci et al. (2016) used "contaminants" dissolved in distilled water, not brine. Popielak et al. (1983) report similar or larger concentrations of "contaminants" (nitrates) than Moraci et al. (2016) while also reporting significant concentrations of chloride and sulfate ions (these species are not present in Moraci et al. 2016 experiments and are expected to result in increased corrosion rates). Thompson et al. (1996) report the maximum corrosion rates between 1 and 3 mm/year. Moraci

et al. (2016) report corrosion rates below about 10^{-4} mm/year, assuming the granular iron surface area of 170 m^2/kg and a mass loss of less than two (2) percent over the testing period. Therefore, corrosion rates in the Delaware Basin are expected to be significantly larger than those reported by Moraci et al. (2016). More details on the Moraci et al. (2016) experiments are provided in response to RPPCR6-Bhperm-3 above.

RPPCR6-Bhperm-6: PRB corrosion test results and Thompson model

A statement in the Executive Summary of Gjerapic et al. (2023, p. iii) indicates that no changes to the existing borehole permeability model are proposed except for the upper limit of degraded borehole permeability. EPA therefore assumes that other elements of the Thompson model, including the depth-related chemical constraints on iron corrosion, are incorporated into the Gjerapic model. If this assumption is correct, please explain how the PRB corrosion test results fit into the effects of depth in the Thompson model. If this assumption is wrong, please provide a detailed description of the Gjerapic model, explaining and justifying any additional differences from the Thompson model.

In Section 2.1, Gjerapic et al. (2023) cite Zeitler (2018a, 2018b) and Roselle (2013) in support of the statement that the intermediate casing in the WIPP repository environment is not likely to fully degrade during the 10,000-year regulatory period under expected mean conditions but may exhibit full degradation under the maximum reported corrosion rates. Further discussion of this statement and its significance to the upper bound permeability of corroded casing are not provided. EPA notes that this statement is consistent with the conclusions of Thompson et al. (1996), that above depths of 300 to 350 m the casing is expected to corrode completely by general corrosion within 200 years but below these depths the corrosion rates may be significantly reduced because of hydrogen fugacity limitations and complete corrosion of iron casing may not occur in 10,000 years. It is not clear that the PRB corrosion results described above, where no depth limitations were imposed by Gjerapic et al. (2023) on their application, are consistent with the depth-dependent conclusions of Thompson et al. (1996).

DOE Response

The Gjerapic et al. (2023) report updates the Thompson et al. (1996) report. In this update, the depth dependence of permeability is retained in acknowledgment of the impacts discussed in the Thompson et al. (1996) model and relevant literature (e.g., Yurtdas et al. 2010, 2011). The depth dependence is reflected in the proposed maximum upper bound permeability. Consequently, the permeability of the lower borehole material is 10 times lower than that of the upper borehole material. However, Gjerapic et al. (2023) do not explicitly discuss the depth dependence of corrosion rates.

The mechanism of steel corrosion described by Thompson et al. (1996) has been tacitly adopted by Gjerapic et al. (2023), except for the radial spalling mechanism proposed by Thompson et al. (1996). Thompson et al. (1996) assumed that “radial diffusion and spallation would reduce the diameter of the plug by half in about 120 years. Such a reduction is deemed sufficient to result in the physical failure of the plug. Based on Bonen (1996), tests on a grout plug that had been in service for over 20 years indicate a cement paste alteration of approximately 1.8 mm from exposed areas. In addition, Matteo and Scherer (2012) suggest that “estimates of the corrosion rate during the flow of carbonated brine in an annulus suggest that the huge neutralization capacity of cement will prevent the acid from causing rapid expansion of small pre-existing

leaks." Even if an annular gap of 10 µm diameter extends along the whole plug of cement, the corroded zone is predicted to advance only a matter of centimeters in a century." Therefore, the revision of the radial spalling mechanism led to a recalculation of the "effective" hydraulic conductivity due to the continuous presence of cement plug materials throughout the 10,000-year performance period. Consequently, Gjerapic et al. (2023) adopted rates of axial spalling and degradation of cement and steel, both in terms of direction and magnitude, following the work of Bonen (1996), Matteo and Scherer (2012), and industry-standard practices, such as those outlined by the National Physical Laboratory (NPL) in 2020.

Like the approach of Thompson et al. (1996), Gjerapic et al. (2023) did not explicitly utilize depth-dependent corrosion rates to calculate the upper permeability bound. Gjerapic et al. (2023) provided a revised upper-bound borehole permeability based on the updated creep model, indicating increased confinement of cement plugs at low stresses. The revised upper bound also considers available site-specific data (Bonen 1996), which indicate limited degradation depth from the exposed surface of the cement plug and estimated rates of degradation/corrosion published in the literature for highly corrosive environments (see, e.g., NPL 2020; ISO 9223). In highly corrosive environments, the maximum annual corrosion/degradation rate is less than 1.0 mm/year, and radial corrosion has a limited impact on the performance of cement plugs (see, e.g., Matteo and Scherer 2012).

To establish a conservative estimate of the upper bound for the borehole permeability, Gjerapic et al. (2023) reviewed corrosion rates reported by Zietler (2018a, 2018b) and Roselle (2013), which are summarized in Tables 4 through 7.

Table 4. Steel Corrosion PA Parameters for CRA 2009 (after Roselle 2013)

Parameter	Units	Description	Probability Distribution	Parameter Value (m/s)
CORRMCO2	m/s	Rate of anoxic steel corrosion under brine-inundated conditions with no CO_2 present	Uniform	Min=0 Max=3.17E-14 Mean=1.585E-14
HUMCORR	m/s	Rate of anoxic steel corrosion under humid conditions	Constant	0

Table 5. Anoxic Steel Corrosion Estimates Based on Roselle (2013)

Rate (m/s)	Rate (m/yr)	Estimated Corrosion after 10,000 yr (m)
1.59E-14	5.00E-07	5.00E-03
3.17E-14	1.00E-06	1.00E-02

Corrosion rates for inundated steel without the presence of carbon dioxide have been undergoing revisions since the original CCA in 1996. For example, the maximum steel corrosion rate of 1.587×10^{-14} m/s used in CCA (1996) was doubled in CRA (2004) and CRA (2009) PA calculations (see Tables 4 and 5) based on the experimental data by Telander and Westerman (1993) reporting increased anoxic steel corrosion

rates at higher pressures. Based on corrosion experiments using WIPP-relevant brines (Roselle 2013), corrosion rates were revised for CRA (2014) and CRA (2019) PA calculations. The most recent PA corrosion parameters used in CRA (2019) are presented in Zietler (2018a, 2018b) and summarized in Tables 6 and 7.

Table 6. Basic Statistics of Anoxic Steel Corrosion Under Brine Inundated Conditions Based on Zeitler (2018a)

	Rate(m/s)	Rate (m/yr)	Estimated Corrosion after 10,000 yr (m)
Mean	1.35E-14	4.26E-07	4.26E-03
Median	1.12E-14	3.53E-07	3.53E-03
Std Dev	1.17E-14	3.69E-07	n/a
Min.	0.00E+00	0.00E+00	0.00E+00
Max	7.92E-14	2.50E-06	2.50E-02

Table 7. Basic Statistics of Anoxic Steel Corrosion Under Humid Conditions Based on Zeitler (2018b)

	Rate(m/s)	Rate (m/yr)	Estimated Corrosion after 10,000 yr (m)
Mean	2.73E-16	8.61E-09	8.61E-05
Median	1.90E-16	5.99E-09	5.99E-05
Std Dev	3.32E-16	1.05E-08	n/a
Min.	0.00E+00	0.00E+00	0.00E+00
Max	1.03E-15	3.25E-08	3.25E-04

Based on the casing geometry (see Drawing 3 in Gjerapic et al. 2023), steel casing may exhibit full degradation under the maximum assumed corrosion rate. However, it is unlikely to fully degrade under average conditions. The geometry of steel casing used by Thompson et al. (1996) is summarized in Table 8. The above consideration assumes that the casing is fully exposed and does not account for the effects of confinement and potential hydrogeomechanical disturbance. One can consider best practices when designing steel structures in aggressive environments to address the potential effects of adverse chemical conditions and hydrogeomechanical disturbance (see, for example, NPL 2020; ISO 9223). The corrosion rate depends on the severity of environmental conditions (see e.g., Mills 1926) and is often expressed as a function of the corrosivity category, as shown in Table 9.

Table 8. Steel Casing Geometry (after Thompson et al. 1996)

Steel thickness	OD (inch)	ID (inch)	Thickness (inch)	Thickness (m)
Surface Casing	13.375	12.615	0.38	0.0097
Intermediate Casing	8.625	7.921	0.352	0.0089
Production Casing	5.5	4.95	0.275	0.0070

Table 9. Corrosion Rates of Metals Based on Environmental Conditions (after NPL 2020)

Corrosivity Category	Corrosion Rates of Metals (μm/yr)			
	Carbon Steel	Zinc	Copper	Aluminum
Very Low	0 – 1.3	0 – 0.1	0 – 0.1	Negligible
Low	1.3 – 25	0.1 – 0.7	0.1 – 0.6	0 – 0.6
Medium	25 – 50	0.7 – 2.1	0.6 – 1.3	0.6 – 2
High	50 – 80	2.1 – 4.2	1.3 – 2.8	2 – 5
Very High	80 – 200	4.2 – 8.4	2.8 – 5.6	5 – 10

Corrosion rates in Table 9 are often used in the design to estimate the sacrificial thickness of steel directly exposed to the atmosphere. When evaluating borehole plug performance, it is essential to consider both the time and direction of exposure. The highest corrosion rates typically occur in structures directly exposed to water and the atmosphere. For steel structures in maritime environments, maximum corrosion rates were typically capped at 0.14 mm/year (BSI 1988; Cowie 2009), a value that agrees favorably with the maximum corrosion rate of 0.2 mm/year reported in Table 9. Extreme corrosion rates for steel structures in specific maritime conditions during the first year of exposure (CX corrosivity category) range from 0.2 to 0.7 mm/year, as per the ISO 9223 standard.

RPPCR6-Bhperm-7: PRB degradation and incomplete degradation

Please explain how the findings of Moraci et al. (2016) for PRB degradation are incorporated into the Gjerapic borehole degradation conceptual model in a manner consistent with the findings of Zeitler (2018a, 2018b), Roselle (2013), and Thompson et al. (1996) that iron at the WIPP repository depth may not be completely degraded in 10,000 years.

EPA found references throughout the Gjerapic et al. (2023) report to studies supporting lower permeabilities for iron corrosion or cement-based grouts derived under conditions that are "less favorable" than the WIPP environment. In this context, the Agency believes the term "less favorable" indicates that Gjerapic et al. believe the WIPP environment would support even lower permeabilities. Such comments were made, for example, about studies by Saiyouri et al. (2011) and Allan and Philippacopoulos (1999). Such references were generally cited without further explanation of how the studies were performed, why conditions at WIPP are more favorable (to even lower permeabilities?- an explanation of what 'favorable' means would help), and in what way are the studies relevant to WIPP. Without this kind of supporting information, it is difficult for the Agency to properly evaluate the significance of these studies as justification for the proposed database change.

Gjerapic et al. (2023, p. 6) cite Popielak et al.'s (1983) report of gypsum and halite precipitation, exsolution of gases under reduced pressures, and wellhead and casing corrosion when testing the brine reservoirs encountered in the vicinity of the WIPP site as evidence of more severe chemical conditions at (or near) the WIPP that could result in lower PRB permeabilities than those measured by Moraci et al. (2016). However, not all boreholes that penetrate the WIPP waste area are postulated in WIPP PA to intersect a brine reservoir and in the interest of establishing an upper bound permeability, chemical conditions that could reasonably support higher permeabilities should be identified and evaluated.

DOE Response

Compared to the WIPP environment, "favorable" refers to resistance to flow. If a particular environment is described as "less favorable," the resistance to flow is expected to be lower. In that case, permeability in this environment is expected to be higher than that of the WIPP borehole. When referring to a change in permeability, a particular environment is considered "less favorable" than WIPP if the rate of change (or reduction) of permeability in this environment is slower than the expected change (or reduction) in WIPP borehole permeability.

Moraci et al. (2016) test solutions are less corrosive than WIPP brines based on the reported concentrations of chlorite and sulfate in Popielak et al. 1983, Table C.2. Popielak et al. (1983) report similar or larger concentrations of nitrates than Moraci et al. (2016) while also reporting significant concentration of chloride and sulfate ions (these species are not present in Moraci et al. 2016 experiments). Additionally, WIPP brines exhibit higher concentrations of suspended solids and greater volumes of gas exsolution. Consequently, the corrosion rates and plugging potential of WIPP brines are expected to be higher than those of solutions used by Moraci et al. (2016). For more details on Moraci et al. (2016) considerations, see the response to RPPCR6-Bhperm-3.

Most of the steel casing providing confinement for the cement plugs, however, is not expected to completely degrade in 10,000 years because of the increased upper borehole confinement (see, for example, Reedlunn et al. 2022) and the anticipated type, direction, and rate of cement degradation (see, for example, Matteo and Scherer 2012) and steel corrosion (see, for example, Subramanian 2008; NPL 2020).

Saiyouri et al. (2011) conducted experiments on poorly graded sand using permeability measurements on cylinders 90 cm in length and 10 cm in diameter. The sand had initial permeability on the order of 10^{-11} m^2 and was then grouted, resulting in a flow structure affected by sand and silt (cement) particles. The grouting process resulted in an overall reduction in permeability and a decrease in the sample porosity. The grouting process is unable to fill the pores between sand grains with 100% efficiency, resulting in a flow network affected by both microporosity (due to the presence of cement or fine-grained components) and mesoporosity (affected by both coarse-grained and fine-grained matrix fractions). After completing the grouting process, Saiyouri et al. (2011) report the permeabilities on the order of 10^{-14} to 10^{-16} m^2, as summarized in Table 10.

Table 10. Permeability Results for Grouted Sands Based on Saiyouri et al. (2011)

Sample	Initial (Pre-Grouting) Permeability (m^2)	Final (Post-Grouting) permeability (m^2)	Initial (Pre-Grouting) Porosity (%)	Final (Post-Grouting) Porosity (%)	Porosity Change (%)
1K1	2.53E-11	1.33E-16	34.2%	20.6%	13.6%
2K2	2.53E-11	1.47E-16	34.2%	20.4%	13.8%
3K1	2.53E-11	6.28E-16	34.2%	20.1%	14.1%
1N	2.51E-11	2.27E-15	34.0%	26.8%	7.2%
2N2	2.51E-11	1.04E-14	34.0%	27.2%	6.8%
3N	2.51E-11	3.10E-14	34.0%	25.6%	8.4%
1C1	1.93E-11	1.40E-14	31.2%	21.7%	9.5%
2C3	1.93E-11	4.90E-14	31.2%	21.8%	9.4%
2C2	1.93E-11	7.69E-15	31.2%	21.8%	9.4%

The cement plugs in the Delaware Basin do not contain sand. Hence, the cement fraction will dominate the flow through those plugs. Consequently, the results of Saiyouri et al. (2011) represent conditions that are expected to yield greater permeabilities than the WIPP conditions. This is because they used uniformly graded materials with larger pore sizes, a significantly larger percentage of sand-sized particles, and a lower percentage of silt-sized particles than the WIPP cement plugs. Hence, one may consider Saiyouri et al. (2011) results as a conservative analog for the upper bound borehole permeability at WIPP, noting that the samples containing a larger percentage of cement (corresponding to a larger change in porosity, e.g., larger than 10 to 12%) are better estimates of the expected upper bound for the borehole permeability. In addition, Sayouri and others' (2011) results in Table 10 demonstrate that even a relatively small percentage (relative to the available pore space) of cement grout will likely reduce the permeability of an initially permeable structure (e.g., when grouting uniformly or poorly graded sands and gravels). Based on the data from Saiyouri et al. (2011) and the above arguments, a reasonable estimate for the upper bound of borehole permeability for cement plugs is 10^{-16} m², ignoring the effects of corrosion degradation and creep.

Allan and Philippacopoulos (1999) reported laboratory permeability measurements for cement-based grouts used in geothermal applications. Their results were influenced by preferential flow along defects caused by shrinkage and debonding of cement and high-density polyethylene (HDPE). The dataset also included measurements on grouts containing sand. Allan and Philippacopoulos (1999) present their data, excluding preferential flow effects, in Table 11.

Table 11. Summary of Allan and Philippacopoulos (1999) Data on Geothermal Grouts without Interface Defects and Debonding

Material/Grout ID	111	114	115	Neat Cement (WC ratio=0.6)
K (cm/s) - grout	1.60E-10	1.60E-10	6.30E-10	n/a
K_max	2.12E-10	1.90E-10	7.00E-10	n/a
K_min	1.08E-10	1.30E-10	5.60E-10	n/a
K (m^2)	1.63E-19	1.63E-19	6.42E-19	n/a
k_max (m^2)	2.16E-19	1.94E-19	7.14E-19	n/a
k_min (m^2)	1.10E-19	1.33E-19	5.71E-19	n/a

Table 12 presents the data of Allan and Philippacopoulos (1999), which include preferential flow effects resulting from the shrinkage and debonding of cement along the smooth HDPE pipe interface.

Table 12. Summary of Allan and Philippacopoulos (1999) Data on Geothermal Grouts with Interface Defects and Debonding

Material/Grout ID	111	114	115	Neat Cement (WC ratio=0.6)
K(cm/s) - U-loop system	1.90E-07	2.40E-07	5.30E-07	7.50E-06
K_max (cm/s)	2.10E-07	3.40E-07	6.70E-07	8.40E-06
K_min (cm/s)	1.70E-07	1.40E-07	3.90E-07	6.60E-06
k(m^2) - U-loop system	1.94E-16	2.45E-16	5.40E-16	7.65E-15
k_max (m^2)	2.14E-16	3.47E-16	6.83E-16	8.56E-15
k_min (m^2)	1.73E-16	1.43E-16	3.98E-16	6.73E-15

Based on the data from Allan and Philippacopoulos (1999) and the expectation of a stronger bond between steel casing and cement than between HDPE pipe and cement, a reasonable estimate for the upper bound of permeability for degraded cement plugs is 10^{-15} m^2. Cement plugs in areas with significant confinement are expected to exhibit lower permeability values.

Proposed upper bound permeability values considered the environmental impacts and chemical conditions that support the fastest corrosion rates in terms of both steel and grout degradation (see Table 9 at the end of the answer to Question No. 6, RPPCR6-Bhperm-6). Boreholes penetrating the repository without encountering a brine reservoir would have a lower corrosion potential. Consequently, the long-term effective hydraulic conductivities would be lower due to the reduced degradation potential of the cement plugs.

Topic 2: Requests related to Gjerapic et al. (2023, Section 2.2) on the hydraulic conductivity of degraded cement, its derivation, and the applicability of the Hazen equation

In the absence of undissolved constituents in the degraded grout, the Agency agrees that the permeability of degraded concrete grout would be expected to be low. However, Gjerapic et al. (2023, p. 8) preface their proposed low-permeability, complete degradation model with the phrase "for

simplicity." The question of complete versus partial dissolution of the grout during the degradation process is important and complex. The presence or absence of undissolved constituents is a key element in assessing the permeability of degraded grout and requires a more substantial technical basis than the approach taken by Gjerapic et al. to estimate an upper bound permeability.

RPPCR6-Bhperm-8: concrete grout degrading to silt-like powders

Please provide a technical justification, including relevant experiments, calculations, and literature citations for the apparent assumption that a completely degraded concrete grout will consist only of silt-like particles represented by cement powders and that no undissolved, coarser degradation products could reasonably be expected to be present that could increase the permeability.

Estimating permeability based on grain size distributions can be associated with considerable uncertainty that is not discussed by Gjerapic et al. (see, for example, Wang et al. 2017). Furthermore, this concern is magnified by the report's application of the Hazen equation to a material that is known to be outside the bounds of its direct applicability.

DOE Response

The Gjerapic et al. (2023) report does not account for the degradation of concrete grouts, which would imply the addition of coarser aggregates to a mixture of cement and water. Instead, the Gjerapic et al. (2023) report proposes conservative upper-bound borehole permeability estimates based on borehole abandonment procedures that follow current industry practice and regulatory guidelines and requirements (see, for example, Gjerapic et al. 2023, Appendix B, Attachment B-2, and Antonio and Romero 2020). Consistent with the PA conceptual model for borehole permeability, the borehole plug material was assumed to degrade, with the upper bound permeability governed by silica gel minerals as the dominant fraction of the cement grout degradation process. The grain size of cement (before the hydration process) and that of the amorphous silica minerals (resulting from the degradation of the cement) can be classified as silt using the standard Unified Soil Classification System. For example, refer to the American Society for Testing and Materials (ASTM) (2020) and the reported particle size distributions, as cited in Ferraris et al. (2004) and Marín et al. (2018).

The initial mixture of the ordinary Portland cement, water, and the potential additives (e.g., soda ash and bentonite) is dominated by a silt-like granular structure reflected in the early permeability of about 10^{-13} m^2 that is being reduced as the cement grout gains strength (see, for example, Backe et al. 1999). The permeability of mature cement pastes is on the order of 10^{-20} m^2 (10^{-13} m/s), as seen, for example, in Christensen et al. (1996). The strength gain is governed by the presence of cement clinker minerals, including tricalcium silicate (alite), dicalcium silicate (belite), tricalcium aluminate (celite), and tetracalcium aluminoferrite (felite). For example, see https://www.cementkilns.co.uk/ckr_phase.html, where the hydration process forms calcium silicate hydrate (CSH), calcium hydroxide (CH), ettringite, and other minerals relevant to cement grout installation (see, e.g., https://precast.org/blog/cement-hydration-kinetics/). During the cement degradation process (see, for example, Grandia et al. 2010), the Ca-Si ratio decreases as Si-enriched phases replace the CSH. These Si-enriched phases vary in composition, with the outer phases consisting of nearly pure silica gel (see, for example, Matteo and Scherer 2012). The zones away from the corrosion zone are dominated by CSH, CH, and other cement minerals. As the cement degrades into Si-enriched phases, the permeability of these phases can be

approximated by considering the flow network dominated by the granulometric distribution of amorphous silica (see, e.g., Marín et al. 2018). For comparison, one can also consider the permeability of the porous matrix, which is governed by the granulometric distribution of cement minerals prior to the hydration process. Assuming the confined state of both hydrated and non-hydrated cement minerals, conservative (upper-bound) permeability estimates can be determined by applying the Hazen equation.

While the chemical degradation of cement grout is expected to result in minerals with the granulometric distribution of silt-like powders (see, for example, Marín et al. 2018 for the grain-size distribution of silica gel), one can envision a mechanical degradation of the corroding steel and cement resulting in larger particle sizes, for example, by sloughing of degraded steel, cement, and the surrounding rock into the open borehole. These larger particles, resulting from material degradation in areas of low confinement, are expected to break down into smaller particles when exposed to creep-induced pressures and continued exposure to the corrosive borehole environment. The breakdown of particles under increasing confining stress is a complex phenomenon (see, e.g., Di Emidio et al. 2009; He et al. 2022), resulting in reduced permeability (see, e.g., Lade et al. 1996; Hattamleh et al. 2013). The cement grout degradation in the areas of high confinement, however, is limited to chemical degradation resulting in calcium dissolution. Matteo and Scherer (2012) note that the exposed (outer) region in direct contact with the corrosive fluid consists of "nearly pure silica gel" (i.e., this zone is not affected by the presence of undissolved constituents).

Note on using Hazen's equation to estimate permeabilities.

While Wang et al. (2017) report considerable uncertainty when estimating hydraulic conductivity values based on the Hazen equation, their research is confined to soil deposits with hydraulic conductivity values larger than about 10^{-5} m/s (10^{-12} m^2). For finer-grained soils, Hazen's equation has been known to overpredict the measured hydraulic conductivity values, i.e., when applying Hazen's equation to soils with the measured hydraulic conductivity values of about 10^{-7} m/s or less, the use of Hazen's equation is expected to result in conservative (larger than measured) hydraulic conductivity estimates. This trend is expected (see, for example, Kozeny-Carman formulation) because finer-grained soils typically exhibit larger surface area and tortuosity than soils for which Hazen's equation was originally developed. More details on the use and applicability of the Hazen equation are provided in the response to RPPCR6-Bhperm-9.

RPPCR6-Bhperm-9: uncertainty in predicted permeability of Hazen equation

Please provide a discussion of the uncertainty associated with the predicted permeability of the Hazen equation for materials that fall within the range of its direct applicability as well as the presumed increased uncertainty when applied to materials outside that range and apply the results to justifying the proposed upper bound permeability for degraded concrete grout.

DOE Response

Hazen's equation is directly applicable to uniform sands with a coefficient of uniformity (Cu) of less than 5. For these soils, hydraulic conductivity predictions based on Hazen's equation are often considered to be accurate to within approximately one order of magnitude. Hazen's equation has been demonstrated to overpredict hydraulic conductivity values for finer-grained

soils such as silty and clayey sands, especially in the lower range of hydraulic conductivity values applicable to silts, for example, a typical hydraulic conductivity value for silts is about 10^{-14} m^2 (10^{-7} m/s), see, for example, Freeze and Cherry (1979). Hence, the use of Hazen's equation to predict the hydraulic conductivity of cement grouts is expected to yield larger-than-expected values. The hydration process is expected to further "skew" the permeability predictions towards higher permeabilities. Thus, the use of the Hazen equation is appropriate for estimating the "upper bound" permeability for the cement plug materials. As the cement grout matures, the permeability prediction based on Hazen's equation should exhibit trends similar to those reported for semi-consolidated sediments. See, e.g., Eggleston and Rojstaczer's (2001) results shown in Figure 1.

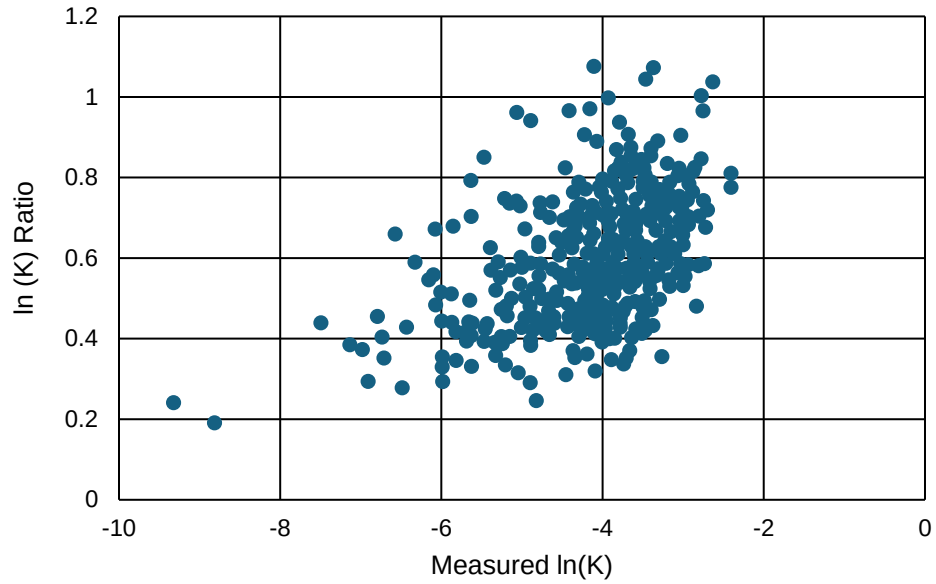

Figure 1. Results from Eggleston and Rojstaczer (2001) – digitized data focusing on outliers of measured permeability values. The ln(K) ratio values < 1.0 indicate an overestimation of ln(K) by Hazen's equation. The hydraulic conductivity data in Figure 1 are expressed in units of cm/s.

As the cement grout hydrates, the permeability decreases. However, even if one discounts the permeability reduction due to hydration (cementation), Figure 1 indicates that the ratio between predicted and measured permeabilities is expected to increase for finer-grained soils characterized by lower permeability values. Consequently, the over-prediction of permeability by the Hazen equation increases as the "effective" grain size (measured permeability) decreases. These trends are illustrated using three (3) selected points in Table 13.

Table 13. Example – permeability overprediction using Hazen equation

Ln K (measured)	Ln K (ratio)	K measured (cm/s)	K_predicted (cm/s)	K_prediction/K_measured
-9.321	0.241	9.0e-5	1.1e-1	1200
-4.897	0.290	7.5e-3	2.4e-1	32
-4.598	0.438	1.0e-2	1.3e-1	13

Note: Reported values based on selected digitized data from Eggleston and Rojstaczer (2001).

The data in Figure 1 can be transformed to allow plotting of the measured hydraulic conductivity values and those predicted by Hazen's equation, as shown in Figure 2.

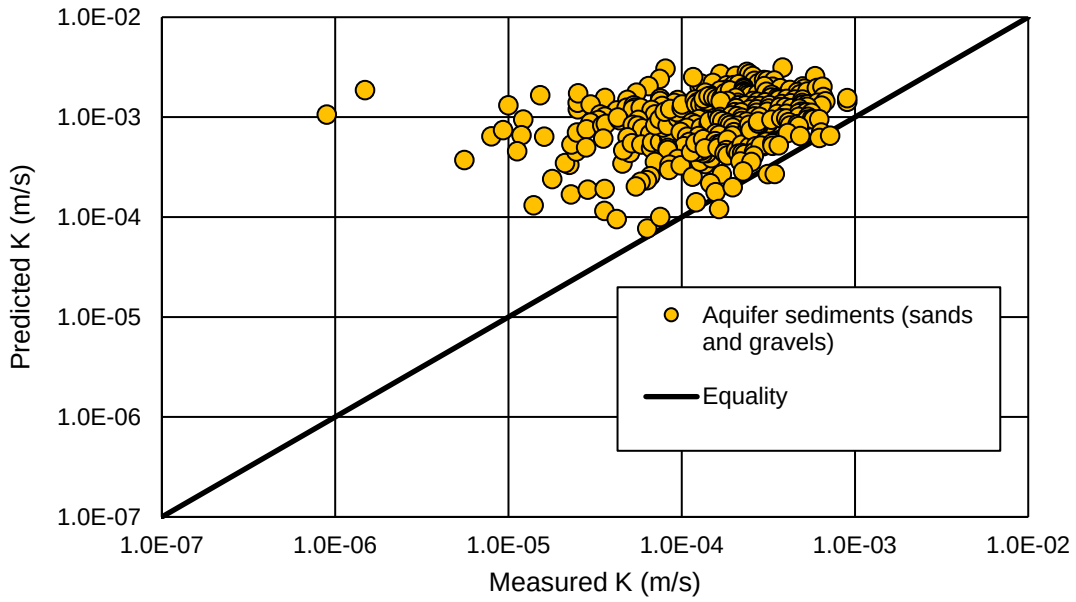

Figure 2. Predicted vs. measured hydraulic conductivity data for semi-consolidated sands and gravels based on Eggleston and Rojstaczer (2001).

Figure 2 demonstrates the expected bias when using Hazen's equation to predict hydraulic conductivity values of granular materials with non-uniform gradation and limited cementation. The values in Figure 2 correspond to semi-consolidated deposits; note that all values above the equality curve indicate an over-prediction of hydraulic conductivities by Hazen's equation. As the hydraulic conductivity of the porous matrix decreases, the Hazen equation is expected to yield a larger deviation from the measured values; that is, the ratio between the predicted and measured hydraulic conductivities is expected to increase as the actual permeability of the porous medium decreases. This trend can be explained by considering the physics of porous flow. Based on the Kozeny-Carman relationship, the hydraulic conductivity value, K, can be expressed as (see, for example, Carrier 2003):

$$K = \frac{\gamma_w}{\mu} \frac{1}{C_{KC}} \frac{1}{S_0^2} \frac{e^3}{1+e} \quad (5)$$

where

γ_w = unit weight of water (N/m^3)
μ = dynamic viscosity of the permeating fluid (Pa s)
e = void ratio
S_0 = specific surface area (1/m)
C_{KC} = Kozeny-Carman constant (typically C_{KC}=5)

After noting that C_{KC} is proportional to tortuosity (where tortuosity is defined as a square of the ratio between the geometric length of the flow path and the straight line across the medium in the direction of flow, see, for example, Corey 1977), one can utilize the finding by Lanfrey et al. (2010) who noted that the tortuosity is inversely proportional to the square of sphericity, ξ, (roundness) of particles (ξ=1 for spheres and ξ<1 for nonspherical particles). Noting that Hazen's equation has been developed for uniform sands, the tortuosity of silt-size mixtures is expected to be higher than that of soils for which Hazen's equation was originally developed. Based on Eq. (5), the soils with larger tortuosity values will exhibit smaller hydraulic conductivities. Therefore, Hazen's equation (developed for uniform sand) overpredicts conductivity for porous media with grain size distributions, such as those found in cement or degraded cement-like mixtures.

In addition, one can consider the theoretical prediction for specific surface area for the pack of spheres with the radius, r,

$$S_0 = \frac{3}{r} \quad (6)$$

Where

S_0 = specific surface for a uniform porous matrix containing spherical particles (m^2/m^3)
r = radius of a spherical particle (m)

Equation (6) demonstrates that the surface area is expected to increase as the "equivalent" radius for uniform sands is replaced with the "equivalent" radius of fine-grained soils. Therefore, Hazen's equation is expected to overpredict the actual hydraulic conductivity of finer-grained soils based on theoretical considerations of flow through porous media, as illustrated by Equation (5). In Hazen's equation, the "equivalent" (hydraulic) radius dependency is captured by the grain size, d_{10}, determined from the particle size distribution curve leading to the hydraulic conductivity, K, expression:

$$K = C d_{10}^2 \quad (7)$$

where d_{10} denotes the particle size below which 10% of the particles are smaller, and C is the empirical constant. The format of the Kozeny-Carman and Hazen relationships defined by Equation (5) and Equation (7) is similar to the equation describing the equivalent hydraulic conductivity, K_{eq}, for an assembly of parallel capillary tubes (see, for example, Corey 1977):

$$K_{eq} = \frac{\phi \gamma_w}{2\mu} \overline{R^2} \quad (8)$$

Where ϕ denotes the porosity and $\overline{R^2}$ represents a weighted mean value of the squared hydraulic radius for N capillary tubes with a radius R_i $(i = 1,2,3, \dots, N)$, defined as

$$\overline{R^2} = \frac{\sum_{i=1}^{N} R_i^4}{\sum_{i=1}^{N} R_i^2} \quad (9)$$

A comparison of Equations (5), (7), and (8) indicates that the $\overline{R^2}$ is approximated by d_{10}^2 in Eq. (7), and by $(e/S_0)^2$ in Eq. (5).

In summary, Hazen's equation is likely to provide an "upper bound" for the porous medium dominated by silt-size particles, especially when considering the expected level of confinement and cementation.

Portland cement-like mixtures are not likely to exceed the hydraulic conductivity of about 10^{-7} m/s as demonstrated by typical values in Table 14 using data from the literature and cement manufacturers (see, e.g., Mentellato et al. 2015 and https://www.breedongroup.com/), assuming medium angularity of the cement particles (see, for example, Carrier 2003; Paine 2019; Loudon 1952) and applying Kozeny-Carman relationship for granular unconsolidated deposits in the form (Corey 1977):

$$K = \frac{\gamma_w}{\mu} \frac{1}{C_{KC}} \frac{1}{S_0^2} \phi^3 \quad (10)$$

where ϕ stands for the flow matrix porosity.

Table 14. Estimated hydraulic conductivity for cement-like mixtures assuming unconsolidated properties and medium angularity of silt-sized particles

Surface Area (m^2/kg)	S_0 (1/m) $\times 10^6$	Specific Gravity (-)	Bulk Density (kg/m^3)	C_{KC} (-)	Porosity (-)	K (m/s) $\times 10^{-7}$
380 - 420	1.2 – 1.3	3.15	1400	7.5	0.556	1.3 - 1.6

As the cement minerals undergo the hydration process, differences (in the ratio) between the predicted and measured permeability values are expected to increase; see, for example, the trends for semi-consolidated deposits in Figure 2. The early cement grout permeability, approximately 10^{-13} m² (10^{-6} m/s), as seen in Backe et al. (1999), continuously decreases as the volume of voids in the pumped slurry is reduced due to the settlement of the cement slurry and the ongoing hydration process. Considering the mature cement paste permeability of approximately 10^{-20} m² (10^{-13} m/s), as seen, for example, in Christensen et al. (1996), the selected upper bound borehole permeability of 10^{-14} m² (10^{-7} m/s) should be viewed as a conservative estimate. The upper bound permeability of 10^{-14} m^2 effectively assumes a complete loss of cementation within the porous matrix due to the removal of calcium. Therefore, while the exact value of the upper bound permeability is difficult to establish, we are confident that 10^{-14} m^2 is a reasonable upper bound borehole permeability.

Topic 3: Requests related to Gjerapic et al. (2023, Section 2.3) on the upper bound permeability of a debris-filled borehole

RPPCR6-Bhperm-10: coarser grained materials in degradation debris and permeability

Please provide copies of any reports or other documentation describing the Phase 1 study of the Electromagnetic (EM) survey performed in 2021 by Zonge International and justifying the selection of the synthetic target depth, thickness, and electrical conductivity used in Phase 1B. The EM survey document provided to EPA in August 2023 is identified as a Phase 1B report and reference is made to a Phase 1 study that assessed the feasibility of detecting deep brine pockets using EM arrays located close to WIPP surface facilities. Please provide a scale plan drawing showing the locations of EM Loops 1, 2, and 3 relative to the projected locations of the underground facilities including the 19 existing and conceptual underground waste panels. The Thompson model for borehole degradation debris includes not only degraded grout and iron corrosion products, but also native material that has sloughed off the walls of the borehole. These native materials, along with other possible insoluble materials and products of incomplete degradation and corrosion, could add a coarser granularity to the debris that was included in the Thompson model (by treating the debris as a silty sand) but does not appear to be included in the Gjerapic model (which appears to ignore the possible presence of coarser grained materials). Please provide justification for the apparent exclusion of coarser grained materials from the degradation debris, or if such materials are assumed to be present, why they would not contribute to higher permeabilities.

> *Gjerapic et al. (2023, p. ii) identify the borehole fill debris as dominated by cement materials with an upper bound permeability on the order of 10^{-14} m^2 when under limited confinement and on the order of 10^{-15} m^2 when under increased confinement. Gjerapic et al. (2023, Section 2.3) therefore conclude that the upper bound permeability of degraded, borehole fill is between 10^{-14} and 10^{-15} m^2. This conclusion is consistent with Gjerapic et al.'s conclusion that the upper bound permeabilities of two constituents of this fill, the corroded iron casing and degraded concrete grout, are both of this same order of magnitude. However, the Gjerapic model appears to ignore other constituents of the degradation debris that were included in the Thompson model.*

DOE Response

The Gjerapic et al. (2023) report does not explicitly specify the percentage of coarser-grained material resulting from the sloughing of rock from the borehole wall, pitting corrosion of the steel casing, and degradation of the cement grout. Instead, the debris occupying the open part of the borehole (borehole annulus) was assumed to contain particle sizes larger than silt and exhibit a relatively high permeability value under low confining pressures.

However, even if one assumes the presence of the degraded, coarse-grained borehole material within the initially open part (annulus) of the borehole and completely neglects the hydraulic resistance from the bottom of the cement plug to the repository, the effective/equivalent borehole permeability (i.e., the permeability assuming homogeneous borehole required for PA calculations) is not likely to exceed 10^{-14} m^2 because of the installed cement plugs (see Answer to Question 4 and the example below). The "effective" borehole permeability is calculated as the harmonic mean of permeability values along the borehole axis and will, therefore, be skewed towards the lowest permeability value. Noting that the degraded cement plugs cannot contain significant amounts of particles larger than silt due to the continuous confinement

(creep) of the borehole, the "effective" permeability is governed by smaller-sized (silt) particles and/or sections of the borehole exhibiting more significant cementation and plugging.

The initial permeability of the degraded borehole debris under low confinement was assumed to be 10^{-10} m^2, one order of magnitude higher than currently assumed in the PA for the degraded borehole material under similar stress conditions. Considering the impenetrability principle (the fact that two objects cannot occupy the same space) and the creep rates predicted by the Reedlunn et al. (2022) model, approximately 200 feet (60 m) of the borehole will be occupied by degrading cement plugs subjected to continuously increasing confining pressures until reaching the stress state before excavation of the borehole. The minimum individual plug length is 100 feet (30 m). The remainder of the borehole, which was left open prior to the installation of the cement plug, will be subjected to gradual creep of the surrounding formation. The increasing confinement of the degraded borehole material within the annulus of the initially open borehole is expected to result in a decrease in overall borehole permeability over time. Assuming a highly corrosive environment that can fully degrade materials within the initially open borehole, materials within the open borehole will be subjected to pore plugging due to salt precipitation and gas exsolution. Even in the most aggressive environments, the effective or equivalent borehole permeability is unlikely to exceed 10^{-14} m². To demonstrate this assertion, one can adopt a set of conservative input parameters:

1. the permeability of a "leaky" cement plug of 6×10^{-16} m^2 (based on the WIPP-specific field data from Christensen and Hunter 1980 determined for a relatively short, 1.8-meter long, "leaky" plug),

2. the plug length, L_{plug}, of 100 feet (30.48 m),

3. depth from the top of the repository to the top of Salado of 400 meters, i.e., L_{eff} = 400 m,

4. permeability of the open borehole of 10^{-10} m^2,

5. neglect the loss of the hydraulic head through the open part of the borehole.

The above inputs allow for the determination of the effective borehole permeability as

$$K_{eff} = K_{plug}\frac{L_{eff}}{L_{plug}} = 6\times10^{-16}m^2\frac{400m}{30.48m} = 7.9\times10^{-15}m^2 \quad (11)$$

For the assumed degradation rate of 0.2 mm/year, the effective borehole permeability after 10,000 years can be calculated as:

$$K_{eff} = K_{plug}\frac{L_{eff}}{L_{plug}} = 6\times10^{-16}m^2\frac{400m}{28.48m} = 8.4\times10^{-15}m^2 \quad (12)$$

RPPCR6-Bhperm-11: relevance of microannuli permeability laboratory results

Please describe the relevance of the microannuli permeability laboratory results of Stormont et al. (2018) to identifying the maximum permeability of a degraded borehole plug at the WIPP.

Gjerapic et al. (2023, Appendix B, p. 8) cite a laboratory study by Stormont et al. (2018) of thermally de-bonded gaps (called microannuli) between the concrete grout and steel casing and report a maximum permeability of 6.7 x 10^{-15} m^2. Since this was a laboratory study that included surface-corroded casing but apparently did not include degraded grout, the relevance of results to the long-term degradation of boreholes at the WIPP is unclear.

DOE Response

The maximum permeability of the degraded borehole depends on the permeability of cement grout, steel casing, and the surrounding rock (borehole components). However, it is also affected by the resistance to flow along the interface areas between these borehole components, including the microannuli between the cement plug and the steel casing.

Assuming the worst-case scenarios in terms of chemical degradation, the borehole plugs are reasonably expected to retain their physical integrity over more than 90 percent of their initial length (see, for example, the expected rates of degradation reported by Bonen 1996 and Matteo and Scherer 2012). As previously noted, the plug's performance depends on the properties of the interface between the cement plug and the steel casing. Hence, the studies by Allan and Philippacopoulos (1999) and Stormont et al. (2018), which include results on hydraulic performance along zones affected by different interface properties, are of significant interest in estimating long-term plug performance. Considering the site-specific WIPP conditions, the effects of plugging, volume expansion of steel (during the corrosion process), creep effects of the surrounding borehole, and gas exsolution are expected to result in lower “effective” permeabilities then measured in experiments accounting for interface conditions in the literature (see, for example, Allan and Philippacopoulos 1999 and Stormont et al. 2018). Incidentally, the estimated magnitude of permeability for “leaky plugs” affected by preferential flow along the steel/cement grout interface is similar to the expected permeability for fully degraded plugs, i.e., areas of the borehole with installed cement plugs where CSH has degraded into amorphous silica compounds. For example, Stormont et al. (2018) report the permeability values between 1.6×10^{-16} and 6.0×10^{-15} m^2 along the corroded casing interface for 0.2m-long laboratory specimens, and Christensen and Hunter (1980) report the in-situ permeability of up to 6.0×10^{-16} m^2 for short (1.8 m-long) “leaky” plugs. The conservative permeability estimates (i.e., values that are likely to overpredict actual permeability values) based on the particle size distribution curves for amorphous silica range from 6.1×10^{-18} to 5.4×10^{-15} m^2, using data from Marín et al. (2018) (see Gjerapic et al., 2023, Appendix B).

The permeability estimates due to the presence of microannuli are not relevant for completely degraded plugs. However, the most reasonable upper bound permeability scenario accounts for the importance of characterizing flow through partially degraded plugs because of the predicted performance of cement grouts by Onofrei et al. (1992), Matteo and Scherer (2012), Bonen (1996), and literature data on the rate of degradation of cement grouts, concrete, and steel (see, for example, Pabalan et al. 2009; Grandia et al. 2010; NPL 2020) demonstrate that the complete plug degradation is not likely to occur during the performance period of 10,000 years. For partially degraded plugs, the existence of microannuli is likely to result in the formation of preferential flow paths. Hence, the upper bound borehole permeability estimates require consideration of the preferential flow through microannuli. Results by Stormont et al. (2018) indicate a range of "effective" permeabilities caused by preferential flow paths (microannuli) due to thermal debonding and corrosion, spanning approximately 10^{-16} to 10^{-14} m^2. Noting that the lower range of "effective" permeabilities corresponds to higher confining stresses, the permeability of 10^{-14} m^2 was assigned to the upper borehole as an upper bound value for both degradation scenarios: 1) scenario assuming a complete degradation of the cement plug and 2) scenario assuming partial degradation of the plug that allows the preferential flow (imperfections) along the steel/cement grout interface. The permeability of 10^{-15} m^2 was assigned to the lower borehole (i.e., the borehole part below the repository), characterized by higher creep rates and higher levels of confinement.

RPPCR6-Bhperm-12: relevance of continuity calculation

Given that the stated objective of Gjerapic et al.'s (2023) analysis is to identify a maximum permeability for loose, degraded borehole fill for the approximately 1,000 m thickness of the salt section and not just the 400 m thickness of the Salado above the repository, please explain the relevance of the continuity calculation (Appendix B, p. 8) to that objective.

In a concluding calculation, Gjerapic et al. (2023, Appendix B, p. 8) assume that the 40 m long Rustler plug has a degraded permeability of 10^{-15} m^2 and that the borehole between that plug and the repository is about 400 m long and is open, providing no resistance to flow. Assuming continuity, the equivalent borehole fill permeability is 1/10th of the plug permeability, or 10^{-14} m^2. Although this calculation appears to be intended to support a conservative maximum permeability of degraded borehole fill of 10^{-14} m^2, it is presented without context to any previously presented scenarios, and it is based on a fraction of the borehole length in question.

DOE Response

In calculating the long-term radioactive releases, the vertical "effective" permeability of the borehole between the repository and the Culebra (the Rustler Formation member with the highest hydraulic conductivity) is of significant interest. This is because it affects both the magnitude of radioactive releases and the response time (i.e., the time required for the radioactive material to reach the Land Withdrawal Boundary). The distance between the repository and the Culebra is approximately 400 meters. For example, one can utilize information in Drawing 1 in Gjerapic et al. (2023) that indicates the top of the WIPP repository at 396.4 meters above mean sea level (amsl) and the bottom of the Culebra at 816.4 m amsl resulting in an effective borehole length of:

$$L_{eff} = 816.4\ m - 396.4\ m = 420\ m \quad (13)$$

If one assumes the plug length of 30 m, the effective borehole permeability, k_{eff}, may be estimated as:

$$k_{eff} = \frac{L_{open}+L_{plug}}{L_{open}/k_{open}+L_{plug}/k_{plug}} = \frac{390m+30m}{390m/10^{-10}m^2+30m/10^{-15}m^2} = 1.4 \times 10^{-14}m^2 \quad (14)$$

The effective permeability presented by Equation (14) may be viewed as the upper bound borehole permeability value because of the following assumptions:

- Limited degradation of the borehole annulus resulting in sloughing and spalling of the borehole cement grout, steel, and surrounding rock into the open borehole.
- Low confinement of the material within the borehole (no creep).
- No plugging and cementation of the borehole material due to the presence of brine fluids and gas exsolution.
- Complete degradation of the cement plug into amorphous silica.

The assumed upper borehole configuration is virtually impossible and may be viewed as an excessively high upper bound value because :

- The maximum degradation rate of a borehole plug is approximately 0.2 mm/year, resulting in about 2 m of degradation over the 10,000-year regulatory period. The degradation length of 2 m is significantly lower than the minimum plug length of 30 m.
- An assumed aggressive environment results in complete degradation of the borehole plug. The assumed permeability of 10^{-15} m^2 implies that the entire plug exhibits permeability of the amorphous silica (see Gjerapic et al. 2023, Appendix B, Section B.3). At the same time, the input parameters for the open borehole assume relatively modest degradation and high permeability of the initially open part of the borehole with a permeability of 10^{-10} m^2.
- It does not account for the effects of borehole confinement due to the rock salt creep.

Similar arguments regarding degradation rates can be extended to the lower borehole. The lower borehole is expected to exhibit a lower permeability than predicted for the upper borehole fill due to higher confinement and faster creep rates. Assuming a modest degradation during the first 200 years, the lower borehole is expected to exhibit a permeability of approximately 10^{-10} m^2 for scenarios that neglect the effects of creeping, and plugging of the porous matrix due to the precipitation of salts and volume expansion of steel during the corrosion process, and sliding along clay seams. Over the 1,200-year period, however, the effects of creep, corrosion, salt precipitation, gas exsolution, and sliding along clay seams are expected to reduce initial permeability values by several orders of magnitude. As noted by Thompson et al. (1996) and Gjerapic et al. (2023), the confinement of the lower borehole fill materials is expected to be significantly larger than for the upper borehole because the confining stress is about 15 MPa (megapascals) at the repository depth (650 m) and about

20 MPa at the mean lower contact of the Salado Formation (860 m). Consequently, the reduction in lower borehole permeability is expected to be more rapid than that in the open areas of the upper borehole (see, for example, Gjerapic et al., 2023, Figures 8, Appendix A, Figures A-14, and A-15). For consistency with the PA calculations (using the reduction of the borehole permeability beneath the repository by one order of magnitude after 1,200 years, see, for example, CRA-2019, Table PA-26), an upper bound permeability of 10^{-14} m^2 was selected for the lower borehole during the period 200 to 1,200 years, whereas 10^{-15} m^2 was selected for the period beyond 1,200 years. The DOE considers these values reasonable because:

- They are consistent with the conceptual model proposed by Thompson et al. (1996), which assumes steel and cement grout degrade within the first 200 years after borehole abandonment.

- Continuity calculations for the upper borehole indicate that k_{eff} is governed by less permeable sections of the borehole. Available laboratory and field data from existing salt mines (e.g., Popp et al. 2018) indicate a relatively rapid rate of self-healing and closure/convergence for openings subjected to increased confinement. Consequently, it is more likely that a single section or several sections of the lower borehole, spanning a 200 m interval in the Salado Formation, will exhibit complete closure. This is particularly relevant to sections where steel and cement grout degrade and slough off toward lower parts of the borehole, or the remaining fill materials are incapable of providing significant backpressure.

- Borehole sections with relatively permeable fill will become less permeable with time due to the volumetric expansion of steel caused by continuous corrosion, salt precipitation, and gas exsolution, which all contribute to the plugging of larger pores.

Topic 4: Requests related to Gjerapic et al. (2023, Section 3) on the application of the new salt constitutive model to estimate the permeability of degraded borehole fill.

RPPCR6-Bhperm-13: description and significance of maximum creep volume loss

Please provide a detailed conceptual description of the development and significance of the maximum creep volume loss of 41.8% for a debris-filled borehole and the segments of the borehole where this conceptual model is applicable.

Instead of calculating the time required for a given porosity reduction as was done in the Thompson model, Gjerapic et al. (2023, p. 12) used the creep closure model to calculate closure rates and decreases in porosity as the maximum creep volume loss was approached. Little description was provided of the conceptual basis for the maximum volume loss.

With the production casing pulled, the open volume of the borehole in the salt section is 41.8% of the total borehole volume. Gjerapic et al. (2023, p. 12) state that the maximum volume loss under salt creep is therefore 41.8% of the initial borehole volume. If it is assumed that all degradation debris that fills the open volume of the borehole in the salt section is from the casing and grout in the salt section, and that no sloughing occurs from above that introduces extra mass, then the increase in porosity from the expanding degradation products would be equal to the fraction of open volume, or 41.8%. The maximum creep volume loss that could occur

would therefore be the loss required to eliminate this extra porosity. This volume loss would restore the degradation products to the porosity of their original, undegraded state. The Agency is uncertain of the accuracy of this conceptual description.

DOE Response

The maximum volume loss due to the creep of the host rock applies to parts of the borehole characterized by an open annulus at the cessation of drilling activities. The PA calculations assume a borehole diameter, D_{bh}, of 12.25 in, consistent with drilling practices at the WIPP depth in the Delaware Basin (see, for example, CRA-2019, Appendix PA-2019, Section PA-2.1.2.1). Assuming the production casing is removed before borehole abandonment, the annulus is defined by the inner/intermediate casing diameter, D_c, 7.921 inches (see Gjerapic et al. 2023, Drawing 3):

$$A_c = \frac{D_c^2 \pi}{4} = \frac{7.921^2 in^2 \pi}{4} = 49.28 \text{ in}^2 \quad (15)$$

Where A_c denotes the open area of the borehole, specifically the area within the intermediate casing. The borehole area, A_{bh}, can be calculated as:

$$A_{bh} = \frac{D_{bh}^2 \pi}{4} = \frac{12.25^2 \pi}{4} = 117.86\ in^2 \quad (16)$$

The amount of open space within the cross-sectional area of the borehole, expressed as a percentage of borehole area prior to creep, can be viewed as a maximum volume loss assuming that the cement grout and steel within the cross-sectional area of the borehole are incompressible:

$$Maximum\ Volume\ Loss = \frac{A_c}{A_{bh}} = 41.8\ \% \quad (17)$$

According to Thompson et al. (1996), the borehole materials are expected to fully degrade within 200 to 5,000 years. Assuming no volume expansion of solid particles of steel or cement grout during the degradation process and incompressible solid particles, the maximum volume loss due to creep is limited to 41.8 percent. This value represents an upper bound for the potential volume loss caused by creep because it assumes:

1. No volume expansion of degraded steel. Corroded steel particles are known to have a larger volume than the original steel (Thompson et al. 1996, Appendix B, Section B.5.4). For example, the volume of magnetite is 2.1 times larger than that of the original steel, whereas ferrous hydroxide occupies a volume 3.73 times larger. Considering the volume expansion of steel during the first 200 years of plug degradation, the initial porosity would be lower than 41.8 percent, and the initial permeability would be less than 10^{-10} m^2.

2. No sloughing of the material located above the borehole cross-section.

3. No reduction in the porosity due to precipitation of salts.

Consequently, the upper bound estimates of 41.8 percent for creep volume loss and 10^{-10} m^2 for the initial permeability were selected to provide a conservative estimate of the time required for the borehole to reach the upper bound permeability values using creep calculations consistent with the approach by Thompson et al. (1996). For the borehole areas exhibiting sloughing of the cement and steel material (towards lower parts of the borehole), the effective permeability reduction and the time for a complete borehole closure is likely to be even faster than predicted by Gjerapic et al. (2023) if one considers a case study reporting a complete closure of mine openings in a potash mine reported by Popp et al. 2018. Finally, the maximum creep volume loss of 41.8 percent agrees favorably with the initial porosity estimated by Thompson et al. (1996) to vary between 25 and 40 percent.

RPPCR6-Bhperm-14: uncertainty associated with predicted permeability using Kozeny-Carman relationship

Please provide a discussion of the uncertainty associated with the predicted permeability of the Kozeny-Carman relationship and its effect on the conclusions of maximum borehole permeability drawn from the salt creep analysis.

Use of the Kozeny-Carman relationship for estimating permeability based on grain size distributions raises Agency concerns similar to those for use of the Hazen equation. Uncertainty can be associated with the Kozeny-Carman relationship that is not discussed by the authors (see, for example, Wang et al. 2017).

DOE Response

Gjerapic et al. (2023) used the same assumptions and calculation methodologies proposed by Thompson et al. (1996) to estimate permeability with the Kozeny-Carman relationship. The Kozeny-Carman relationship assumes a porous medium can be conceptualized as an assembly of capillary tubes creating a network of interconnected channels. As a result, fluid particles flowing through granular porous media follow a sinuous (tortuous) path (Corey 1977). The Kozeny-Carman relationship is typically applied to granular soils, including non-plastic silts (see, for example, Carrier 2003). The Kozeny-Carman relationship is semi-empirical in its nature because the Kozeny-Carman coefficient, C_{KC}, in Equation (18) is a function of the soil type affecting the estimated hydraulic conductivity:

$$K = \frac{\gamma_w}{\mu}\frac{1}{C_{KC}}\frac{1}{S_0^2}\frac{e^3}{1+e} = \frac{\gamma_w}{\mu}\frac{1}{C_{KC}}\frac{1}{S_0^2}\frac{\phi^3}{(1-\phi)^2} = \alpha\frac{\phi^3}{(1-\phi)^2} \quad (18)$$

where:

γ_w = unit weight of water (N/m^3)
μ = dynamic viscosity of the permeating fluid (Pa s)
e = void ratio
ϕ = porosity (-)
S_0 = specific surface area (1/m)
C_{KC} = Kozeny-Carman constant

For uniform sands consisting of rounded (semi-spherical) particles, the Kozeny-Carman coefficient, $C_{KC} = 5$ (see, e.g., Carrier 2003; Corey 1977). Similarly to the application of Hazen's

equation (see Answer No. 9 above), the Kozeny-Carman equation is expected to overpredict the hydraulic conductivity/permeability of finer-grained soils unless the coefficient C_{KC} or α In Equation (19), the parameters are recalibrated.

Gjerapic et al. (2023) assumed the initial borehole permeability of 10^{-10} m^2 for a degraded section of the open borehole prior to being affected by creep. This condition corresponds to the initial hydraulic conductivity of about 10^{-3} m/s assuming the percolating fluid properties of $\gamma_w = 9.8kN/m^3$, $\mu_w = 0.001\ Pa\ s$. For these degraded borehole conditions, representing hydraulic properties 200 years after abandonment, Gjerapic et al. assigned a porosity of 41.8 percent. From Equation (18), one can determine the α value as

$$\alpha = K\frac{(1-\phi)^2}{\phi^3} = 10^{-3}m/s \times \frac{(1-0.418)^2}{0.418^3} = 4.638 \times 10^{-3}m/s \quad (19)$$

For the assumed values of γ_w, μ_w and C_{KC}, one can now calculate the corresponding specific surface area, e.g.

$$S_0 = \sqrt{\frac{\gamma_w}{\mu_w \alpha}\frac{1}{C_{KC}}} = \sqrt{\frac{9800N/m^3}{0.001Pas \times 4.636 \times 10^{-3}}}\sqrt{\frac{1}{5}} = 2.06 \times 10^4\ m^{-1} \quad (20)$$

The specific surface area is often expressed in m²/kg units, i.e., normalized by the density of solid particles. For the assumed particle density, $\rho_s = 2700\ kg/m^3$, one can determine the specific surface area by mass, S_{0m}:

$$S_{0m} = \frac{S_0}{\rho_s} = \frac{2.06 \times 10^4 m^2/m^3}{2700kg/m^3} = 7.6\ m^2/kg \quad (21)$$

For the uniform (monodispersed) porous matrix comprised of spherical particles with a diameter, d_m, one can calculate the specific surface area as

$$S_0 = 6/d_m \quad (22)$$

Equation (22) can be used to evaluate the specific surface area as a function of grain size diameter for different particle sizes, based on the Unified Soil Classification System (see, e.g., ASTM 2487, 6913, and 7928). The calculated specific surface, hydraulic conductivity, and permeability estimates using Equation (18), for different particle sizes are summarized in Table 15. Values in Table 15 were determined for a uniformly graded matrix with a porosity of 41.8 and assuming water as a percolating fluid:

Table 15. Specific surface area and KC hydraulic conductivity estimates as a function of the (spherical) particle size diameter for uniform/monodisperse porous matrix

Particle Size	Sieve Size No.	d_m, max (mm)	S_0 (1/m)	S_{0m} (m^2/kg)	C_{KC} (-)	K (m/s)	k (m^2)
Coarse Sand	4	4.75	1.3×10^{3}	4.7×10^{-1}	5	2.7×10^{-1}	2.7×10^{-8}
Medium Sand	10	2	3.0×10^{3}	1.1	5	4.7×10^{-2}	4.8×10^{-9}
Fine Sand	40	0.425	1.4×10^{4}	5.2	5	2.1×10^{-3}	2.2×10^{-10}
Silt	200	0.075	8.0×10^{4}	3.0×10^{1}	5	6.6×10^{-5}	6.7×10^{-12}
Clay	n/a	0.002	3.0×10^{6}	1.1×10^{3}	5	4.7×10^{-8}	4.8×10^{-15}

The specific surface values in Table 15 are not realistic for naturally formed deposits. For example, Pennel (2016) reports a specific surface area for soils ranging from less than 100 to more than 8×10^5 m^2/kg. Yan et al. (2023) report specific surface areas for clayey soil deposits between 6×10^3 and 4.4×10^5 m^2/kg. The soil with the smallest surface area, reported by Yan et al. (2023), contained a relatively low percentage of fines, which refer to silt and clay-size soil particles passing through the No. 200 sieve (i.e., particles with an effective diameter smaller than 75 microns). This sample consisted of 96 percent and-size particles and 4 percent fines, with a corresponding specific surface area of 6×10^3 m^2/kg.

It is of interest to investigate the range of specific surface area values reported for the degraded borehole materials, cement, and steel. After hydration, the cement grout is likely to exhibit a specific surface area of more than 4×10^3 m^2/kg (see, e.g., Odler 2003). Prior to hydration, one can estimate the specific surface area from the reported values for the Ordinary Portland Cement (OPC). Mentellato et al. (2015) report the specific surface area for the OPC is more than 400 m2/kg, which agrees well with the manufacturing data, see, e.g., Breedon (2024). Diaz-Mateus et al. (2024) report a specific surface area of 5.41×10^3 m^2/kg for steel corrosion products (magnetite). For the long-term borehole porosity of 32 percent specified in the PA (see, e.g., CRA 2019, Table, PA-22), a range of conservative borehole permeability estimates can now be calculated for S_{0m} values between 400 and 4000 m^2/kg and the OPC particle density of 3000 kg/m^3 as shown in Table 16.

Table 16. KC hydraulic conductivity and permeability estimates as a function of the surface area for degraded borehole materials assuming uniform/monodisperse porous matrix

Material Condition	ϕ (-)	S_0 (1/m)	S_{0m} (m^2/kg)	C_{KC} (-)	K (m/s)	k (m^2)
Loose (unhydrated) Cement	0.32	1.2×10^{6}	400	5	9.7×10^{-8}	9.8×10^{-15}
Hydrated Cement	0.32	1.2×10^{7}	4000	5	9.7×10^{-10}	9.8×10^{-17}

The degraded borehole materials within the borehole are not likely to be uniformly graded, may exhibit a more tortuous path than predicted by the Kozeny-Carman equation, and are likely to

contain particles of different shapes and sizes. Hence, the value of the Kozeny-Carman constant, C_{KC}, may be adjusted to account for the presence of smaller (silt-size) particles (see, e.g., Carrier 2003), different particle shapes (see, e.g., Lanfrey et al. 2010), and more tortuous paths (see, e.g., Clennell 1997). Any of these adjustments would lead to an increase in the C_{KC} value and a further decrease in the corresponding hydraulic conductivity, leading to less conservative (lower) borehole permeability upper bound estimates than those reported in Table 16.

The permeability values in Table 15 and Table 16 represent conservative upper bound estimates for a uniformly graded porous matrix with relatively high porosity. Natural soils exhibit a range of particle sizes, with smaller particles often obstructing the flow through the porous network formed by larger particles. Furthermore, the flow through larger geological formations may be influenced by structural features (e.g., fractures) that are not present at smaller scales. The flow through the intrusion borehole will be strongly affected by sections with the lowest permeability along the vertical flow path. Therefore, it is reasonable to evaluate the borehole permeability upper bound by considering values from the geotechnical literature, which utilizes both laboratory and field-scale data for the design of engineering structures (e.g., USBR 1987; Bardet 1997). Available permeability data, including measurements and calibration efforts on geological and larger scales (e.g., Freeze and Cherry 1979), may be used as a secondary resource. The range of hydraulic conductivity and permeability data for various soil types, based on values reported by Bardet (1997), is summarized in Table 17.

Table 17. Hydraulic conductivity and permeability estimates based on geotechnical literature (after Bardet 1997 using data from Kulhawy and Mayne 1990 and Terzaghi and Peck 1967)

Soil Type	K (m/s)	k (m^2)
Gravel	$> 10^{-3}$	$> 10^{-10}$
Sandy gravel, clean sand, fine sand	10^{-3} to 10^{-5}	10^{-10} to 10^{-12}
Sand, dirty sand, silty sand	10^{-5} to 10^{-7}	10^{-12} to 10^{-14}
Silt, Silty Clay	10^{-7} to 10^{-9}	10^{-14} to 10^{-16}
Clay	$< 10^{-9}$	$< 10^{-16}$

Borehole permeability values are likely to be affected by the presence of bentonite, which is typically added to cement grout and drilling mud (see, e.g., Antonio and Romero 2020; Vipulanandan and Mohammed 2020). Additionally, sections of the borehole may be affected by degraded rock mass containing claystone and mudstone minerals. Considering that the permeability values in Table 17 refer to soils at confining pressures that are significantly lower than expected at the WIPP site (e.g., typical stress levels for standard geotechnical applications are below 0.1 to 0.2 MPa while borehole stresses in the Salado exceed 5MPa), accounting for the corrosive environment that is likely to lead to cementation and plugging due to the precipitation of salts, the tendency of the rock salt to creep and “heal” the existing fractures and openings (see, e.g., Popp et al. 2018) as well as provide continuous confinement, the KC model selected for creep calculations by Gjerapic et al. (2023) is expected to yield conservative estimates in terms of the borehole closure and the predicted time required to reach the upper bound hydraulic conductivity value of 10^{-15} m^2. Specifically, the α value featured in Equation (19) is expected to undergo a significant reduction because both the tortuosity and the specific

surface area of the borehole fill material are likely to increase with time as the porosity (the volume of pores) decreases.

Wang et al. (2017) considered relatively coarse unconsolidated sediments with a hydraulic conductivity range of 10^{-5} to 10^{-3} m/s. Therefore, the data from their study are not applicable to silty materials, which are expected to dominate the borehole hydraulic performance. In terms of the uncertainty of predicted values, the reported data indicate a scatter of approximately one order of magnitude around the proposed regression lines for all predictive formulations considered by Wang et al. (2017), including the Kozeny-Carman relationship.

The trend for the capillary tube flow models to overpredict the permeability of soils with finer grain size distribution is expected based on the expected increase in tortuosity (resulting in larger values of the C_{KC} parameter as the degree of the particle "sphericity" decreases, see Lanfrey et al. 2010) as well as the increase in the specific surface area (ϕ/S_0 is proportional to the "equivalent" hydraulic radius). As expected, this trend is similar to Hazen's equation (see answer to question RPPCR6-Bhperm-9). Hence, the magnitude of the permeability overprediction (e.g., as defined by the ratio $k_{predicted}/k_{measured}$) is expected to increase as the "effective" grain size of the soil (and the corresponding permeability) decreases, as shown by a comparison between the modified Kozeny-Carman equation proposed by Carrier (2003) and reported by Pap and Mahler (2021) in Figure 3.

Figure 3 shows that the typical scatter around the mean for measured permeability values is smaller than the magnitude of overprediction by the modified Kozeny-Carman relationship. For K > 10^{-7} m/s or lower, i.e., for permeability values below 10^{-14} m^2 (assuming water as a percolating/reference fluid), the Kozeny-Carman model is expected to consistently overpredict measured permeability values (assuming the calibration of model parameters for uniform sands, i.e., the calibration range of hydraulic conductivities between 10^{-5} and 10^{-3} m/s).

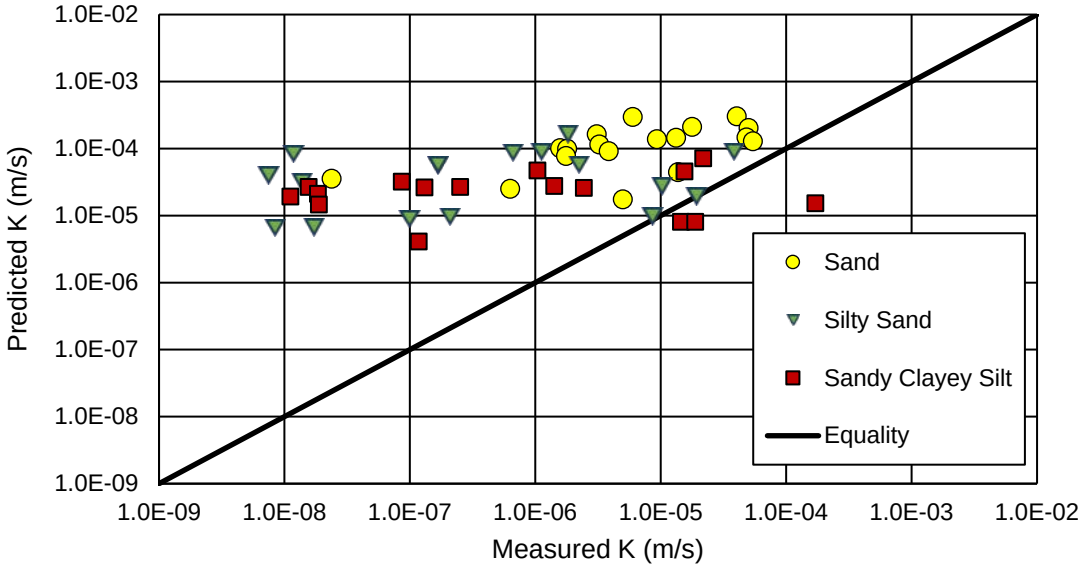

Figure 3. Measured vs. predicted hydraulic conductivity data for unconsolidated soils after Pap and Mahler (2021). Predicted Ks above the 1:1 line were calculated by Pap and Mahler (2021) using the Modified Kozeny-Carman equation of Carrier (2003).

Note that the α value in Eq. 19 was calibrated for a relatively large porosity of 41.8 percent and a corresponding permeability value of 10^{-10} m^2. Therefore, application to lower porosities is expected to result in an overprediction, especially for *K* values that are several orders of magnitude lower than the initial 10^{-3} m/s. Hence, the modeling approach adopted by Thompson et al. (1996) and utilized by Gjerapic et al. (2023) is expected to consistently overpredict the borehole K at larger times. This is due to the initial hydraulic conductivity being reduced by 2 to 3 orders of magnitude. The uncertainty of the K_0-value using the KC model prediction is within one order or magnitude.

RPPCR6-Bhperm-15: explanation and timeline of the conceptual model for surface hole, upper salt section, and lower salt section

Please provide a summary explanation and timeline of the Gjerapic conceptual model for borehole degradation and subsequent compression for a) the surface hole; b) the upper salt section borehole above the repository; and c) the lower salt section borehole below the repository.

DOE Response

The timeline of a conceptual model for the surface hole, upper salt section, and lower salt section follows the assumptions proposed by Thompson et al. (1996). This approach retains conservatism and assures consistency with the current implementation of the borehole permeability model in PA calculations. For the first 200 years, both upper and lower boreholes are assumed to remain open while the cement plugs remain intact. After 200 years, the steel and cement in the borehole are assumed to degrade, generating infill for both the upper and lower sections of the borehole. The infill is subjected to the creep of the surrounding rock and changes in the hydrogeochemical conditions within the borehole. These combine to change borehole permeability over time. The infill in the lower borehole is subjected to higher confining stress and, therefore, exhibits a lower long-term permeability than the upper borehole infill after 1,200 years. The conceptual model timelines are summarized in Table 18.

Table 18. Timeline of the conceptual model for the degradation of the surface hole, upper salt, and lower salt sections, along with the corresponding upper bound permeabilities.

Years After Abandonment	Surface Hole[1,3,4]	Upper Salt Section[2,3]	Lower Salt Section
0 to 200	$1.6\times10^{-16}m^2$	$1.1\times10^{-16}m^2$	$10^{-9}m^2$
200 to 1200	$10^{-11}m^2$	$10^{-14}m^2$	$10^{-14}m^2$
> 1200	$10^{-11}m^2$	$10^{-14}m^2$	$10^{-15}m^2$

1) The surface hole is assigned a length of 250 m, with a surface plug length of 15.76 m, as per CRA-2019, Appendix PA, Table PA-26, and Figures PA-12 to 14.
2) The upper salt section is assigned a length of 400 m, as per the Los Medaños plug length of 36 m, as stated in CRA-2019, Appendix PA, Table PA-26, and Figures PA-12 to 14.
3) Effective borehole permeabilities for the first 200 years after abandonment were determined for an open borehole permeability of 10^{-9} m^2 and a plug permeability of 10^{-17} m^2 per CRA-2019, Appendix PA, Table PA-26.
4) Surface hole permeability was not evaluated by Gjerapic et al. (2023). Values were adopted from Thompson et al. (1996).

For the first 200 years after abandonment, effective permeability for the surface hole and upper salt section was determined from the equation:

$$k_{eff} = \frac{L_{open}+L_{plug}}{L_{open}/k_{open}+L_{plug}/k_{plug}} \quad (23)$$

RPPCR6-Bhperm-16: sample calculations using the Kozeny-Carman method

Please provide sample calculations showing application of the Kozeny-Carman method used to develop the curves shown in Figures 7 and 8 of Gjerapic et al. (2023), specifically including calculation of a permeability of 10^{-15} m^2.

DOE Response

Gjerapic et al. (2023) calculated borehole hydraulic conductivity, K, as a function of the average porosity, ϕ, using the Kozeny-Carman relationship:

$$K = \alpha\frac{\phi^3}{(1-\phi)^2} \quad (24)$$

In Eq. 24, the initial hydraulic conductivity, K_0, was set to 0.001 m/s (0.1 cm/s), assuming α = 0.463 cm/s and an initial porosity, ϕ_0, of 41.8 percent. The ϕ_0 value was selected based on the borehole geometry (see the response to RPPCR6-Bhperm-13), and the α value was determined from the K_0 value as follows:

$$\alpha = K_0\frac{(1-\phi_0)^2}{\phi_0^3} \quad (25)$$

Assuming a borehole diameter, D_{bh}, of 12.25 inches (0.31 m)[1] and an inside casing diameter of 7.92 inches (0.20 m), the borehole volume per unit length, V_0, was determined to be 7.604×10^{-2} m^3/m with a corresponding volume of solids (steel and cement grout), V_s, of 4.425×10^{-2} m^3/m. It was assumed that the volume of solids (steel and cement grout) remains constant during the creep deformation process. As the borehole diameter changes due to creep, the borehole volume per unit length is calculated as:

$$\mathrm{V(t)} = \frac{D(t)^2\pi}{4} \quad (26)$$

The volume loss is calculated as:

$$\Delta V = \frac{V_0-V(t)}{V_0} \quad (27)$$

The resulting pore volume is then calculated using:

[1] The PA calculations assume the borehole diameter of 12.25 inches consistent with drilling practices at the WIPP depth in the Delaware Basin (see, for example, CRA-2019, Appendix PA-2019, Section PA-2.1.2.1).

$$V_p = V(t) - V_s \quad (28)$$

The corresponding porosity is then given by:

$$\phi = \frac{V_p}{V(t)} \quad (29)$$

This porosity is used to determine *K* using Eq. 24 and the corresponding permeability according to:

$$k = K \frac{\mu}{\gamma_w} \quad (30)$$

where μ is the dynamic viscosity of the fluid and γ_w is the fluid unit weight. For freshwater at 25°C, μ=0.001 Pa s and γ_w =9.8 kN/m^3, the borehole hydraulic conductivity and permeability values are derived from Eq. 24 and Eq. 30 and are summarized in Table 19.

Table 19. Borehole permeabilities derived from the Kozeny-Carman Equation.

D_{bh} (m)	V_{bh} (m^3/m)	ΔV (%)	V_p (m^3/m)	ϕ (-)	K (cm/sec)	k (m^2)
0.311	0.0760	0.00%	0.0318	0.4181	1.0E-01	1.0E-10
0.300	0.0707	7.04%	0.0264	0.3740	6.2E-02	6.3E-11
0.295	0.0683	10.11%	0.0241	0.3527	4.8E-02	4.9E-11
0.290	0.0661	13.13%	0.0218	0.3301	3.7E-02	3.8E-11
0.280	0.0616	19.02%	0.0173	0.2814	2.0E-02	2.0E-11
0.270	0.0573	24.70%	0.0130	0.2272	9.1E-03	9.3E-12
0.265	0.0552	27.46%	0.0109	0.1978	5.6E-03	5.7E-12
0.264	0.0547	28.01%	0.0105	0.1917	5.0E-03	5.1E-12
0.260	0.0531	30.18%	0.0088	0.1666	3.1E-03	3.1E-12
0.250	0.0491	35.44%	0.0048	0.0986	5.5E-04	5.6E-13
0.240	0.0452	40.50%	0.0010	0.0220	5.1E-06	5.2E-15
0.239	0.0448	41.05%	0.0006	0.0129	1.0E-06	1.0E-15

RPPCR6-Bhperm-17: Applicability of Kozeny-Carman model for fine-grained borehole degradation debris.

Please provide a justification for the apparent assumption that the Kozeny-Carman model for estimating permeability reductions resulting from porosity reductions is applicable to the fine-grained borehole degradation debris expected in the Gjerapic conceptual model and is valid for the very low permeabilities and steep permeability declines depicted in Gjerapic et al. (2023, Figure 8).

DOE Response

Gjerapic et al. (2023) used the Kozeny-Carman model to estimate borehole permeability as the degraded cement grout and steel debris deform under creep pressures. This assertion is based on a relatively high value assumed for the initial borehole permeability (i.e., the undeformed

borehole permeability was set to 10^{-10} m^2, a typical value for uniformly graded materials characterized by relatively large particle sizes, and a single order of magnitude lower than the permeability of an open borehole of 10^{-9} m^2 assumed for PA calculations). Consequently, the initial α parameter used for Kozeny-Carman calculations was fitted to field conditions representing porous matrix with large pore diameters.

The Kozeny-Carman equation used by Thompson et al. (1996) and Gjerapic et al. (2023) can be written as:

$$K = \frac{\gamma_w}{\mu}\frac{1}{C_{KC}}\frac{1}{S_0^2}\frac{e^3}{1+e} = \frac{\gamma_w}{\mu}\frac{1}{C_{KC}}\frac{1}{S_0^2}\frac{\phi^3}{(1-\phi)^2} = \alpha\frac{\phi^3}{(1-\phi)^2} \quad (31)$$

where:

γ_w = unit weight of water (N/m^3)
μ = dynamic viscosity of the permeating fluid (Pa s)
e = void ratio
ϕ = porosity (-)
S_0 = specific surface area (1/m)
C_{KC} = Kozeny-Carman constant

The results of Equation (31) are determined for the alpha parameter calibrated under the assumption of large pore sizes (large hydraulic conductivity values). Consequently, the results obtained from the Kozeny-Carman relationship, Equation (31), are expected to overpredict actual permeability values because the flow tortuosity and the specific surface area will increase with time. Parameter C_{KC} in Equation (31) is proportional to tortuosity, and the surface area of the degraded borehole material will increase due to the crushing of larger particles and precipitates deposited within the porous matrix. Therefore, the Kozeny-Carman model is expected to consistently overpredict the actual borehole *K*-value at larger times, as the initial hydraulic conductivity is reduced by 2 to 3 orders of magnitude or more, i.e., at times when the presence of finer-grained material and steeper permeability declines will govern the borehole permeability.

Additional arguments for the applicability of the Kozeny-Carman equation to finer-grained material (e.g., non-plastic silts) may be found in Carrier (2003) and the DOE's responses to RPPCR6-BHPERM-9 and RPPCR6-BHPERM-14 above.

Topic 5: Questions relating to the effects of backpressure on closure rates

In its review, EPA combined several tables for Case 3 found in Gjerapic et al. (2023), which are based Reedlunn et al.'s (2022) creep closure model, into a summary table (Table 1 below). Case 3 simulates the greatest backpressure and results in the slowest creep closure rates and permeability reductions, which can help bound a maximum permeability.

Table 1. Time (Years) Required to Reach Permeability Reductions at Specified Borehole Depths for Castile Brine Reservoir (Case 3) Backpressures. Permeability reduction times from Gjerapic et al. 2023, Tables A-4 through A-7. Maximum closure times from Gjerapic et al. 2023, Table A-3. Note that 200 years should be added to each of the times in the table to account for the initial period before general corrosion is assumed to be complete.

k/ko	250 m Depth	450 m Depth	650 m Depth	850 m Depth
1×10^{-1}	3,779	756	329	176
1×10^{-2}	5,732	1,144	500	269
1×10^{-3}	6,681	1,331	583	314
1×10^{-4}	7,130	1,419	622	335
1×10^{-5}	7,341	1,466	640	346
1×10^{-6}	7,409	1,509	649	356
Maximum Closure	7,523	1,500	656	354

Under the Thompson model assumption that general corrosion occurs above depths of 300 to 350 m, after 200 years the casing and grout have completely degraded and back pressure is only from borehole fill. Thompson et al. (1996, p. D-2) concluded that it is not unreasonable to ignore this backpressure because it would be small for closures up to the maximum of 23% needed to achieve a one order of magnitude decrease in permeability. They also state that ignoring backpressure will probably not be reasonable for closures larger than 23% and concluded that "… additional closure will be increasingly resisted, making it likely that the one order of magnitude reduction in permeability from the effects of creep used here will not be exceeded with additional time." (Thompson et al. 1996, p. D-2). RPPCR6-Bhperm-18: initial permeability of degraded borehole debris used in creep closure analysis

This conclusion suggests that recovery of the maximum borehole volume loss of 41.8% in the Gjerapic model may not be physically achievable because backpressure from the consolidating borehole fill may exceed the applied confining stress from salt creep, particularly at shallower depths. If this conclusion is correct, the permeability loss in the Gjerapic model may be limited to one, or perhaps two orders of magnitude instead of the five or six orders of magnitude shown in Table 1. If the permeability reduction cannot reasonably exceed one or two orders of magnitude in the Gjerapic model, the permeability would decrease under salt creep from $10^{-10} m^2$ to 10^{-11} or $10^{-12} m^2$, which are of the same order of magnitude as the maximum permeability assumed in the Thompson model.

RPPCR6-Bhperm-18: initial permeability of degraded borehole debris used in creep closure analysis.

Please explain the technical basis for the initial permeability of 10^{-10} m^2 assumed for the degraded borehole debris in the creep closure analysis.

DOE Response

The creep closure analysis by Gjerapic et al. (2023) adopted the methodology and assumptions from Thompson et al. (1996) and focused on the borehole section with an open annulus. According to Thompson et al. (1996) and the current Performance Assessment (PA) based on the peer-reviewed conceptual model for exploration boreholes, the degraded borehole is filled with silty-sand-like material after 200 years (see DOE, 2019, Section PA-2.1.2.5 and DOE, 1996, Appendix PEER 1). In their analysis, Gjerapic et al. (2023) considered WIPP-specific conditions and current practices in evaluating the degradation of borehole materials. It was concluded that the complete degradation of borehole materials, which could generate particles larger than silt, is possible only within the borehole section without a cement plug.

Based on this analysis, the degraded material in the initially open annulus was assigned a permeability of 10^{-10} m^2. This is the maximum reported permeability for a manufactured porous

medium comprising granular iron (e.g., TAPRBI 2002). The 10^{-10} m^2 value has also been used by Grandia et al. (2010) to model the degradation of cement grouts in fractured media under low confining pressures. Hence, Gjerapic et al. (2023) adopted this value as the upper bound of the initial permeability for degraded borehole fill.

RPPCR6-Bhperm-19: The Effect of Backpressure Buildup on Permeability Reductions in Updated Modeling.

Thompson et al. (1996, p. D-2) stated that backpressure buildup from the consolidated borehole fill makes it likely that one order of magnitude reduction in permeability due to salt creep would not be exceeded with additional time. Please describe the effect of backpressure buildup on the reductions in permeability determined from the updated modeling described in Gjerapic et al. (2023, Section 3.1) and provide justification that a reduction of five or six orders of magnitude is possible.

This second question asks how the results should be used. There are two interrelated elements to this question. How should the creep closure rates in salt be considered in PA and how should an initial, degraded borehole permeability be selected as a starting point for that closure?

DOE Response

Based on Reedlunn et al. (2022), the creep rates of the Salado Formation may result in relatively rapid borehole closure. Similarly, creep rates are expected to confine the installed borehole plugs significantly. The exposure of borehole materials to WIPP brines represents an adverse environmental condition in terms of the potential for steel corrosion and cement degradation. Consequently, following the current conceptual model for borehole degradation, the effective borehole permeability 200 years after borehole abandonment will be lower than the initial permeability of the open borehole[2]. Selecting the initial permeability for a section of the open borehole in the Salado Formation, however, is a difficult task because the effective borehole permeability varies from essentially zero (e.g., for parts of the borehole that are exhibiting complete closure due to sliding along the clay seams, see, for example, Wagner and Hillesheim 2009) to 10^{-9} m^2 (e.g., for "open"/unobstructed section of the borehole that are not exhibiting significant degradation). Hence, a conservative estimate of the initial borehole permeability, 10^{-10} m^2, was selected by Gjerapic et al. (2023) as an "effective" permeability for the open parts of the borehole (borehole sections outside the plug installation area) before initiating creep calculations. Based on the hydrodynamic, chemical, and geomechanical conditions, different sections of the borehole may experience different back pressures depending on:

- the magnitude of pore pressures exerted by brine and gas;
- the rate of degradation;
- the amount of degraded material within the open borehole section;
- the amount of precipitates within the borehole annulus and the matrix of degraded material;

[2] In PA calculations, the open borehole permeability is set to 10^{-9} m^2.

- the degree of compaction of borehole material;
- geological conditions of the rock mass (e.g., clay seams) along the borehole axis.

Thompson et al. (1996) suggested that backpressure is unlikely to have a significant effect on creep closure for closures up to 23 percent. For closures > 23 percent, Thompson et al. (1996) emphasized the importance of considering the backpressure of the borehole fill. Due to the complexity of accounting for the coupled hydrodynamic, mechanical, and chemical mechanisms necessary for an accurate evaluation of backpressure in the borehole annulus, Thompson et al. (1996) conducted creep calculations without considering backpressure effects. In their analysis, it was assumed that the pore pressures within the borehole resembled hydrostatic conditions, using a brine unit weight of 11.8 kN/m³.

Similar calculations were performed by Gjerapic et al. (2023), with the backpressure varying from zero (Case 1) to hydrostatic (Case 2) and applying the WIPP-12 excess pore pressures within the borehole annulus (Case 3) throughout the performance period. Neither the Thompson et al. (1996) nor Gjerapic et al. (2023) analyses consider the effects of volume expansion due to steel corrosion, pore plugging to gas exsolution and salt precipitation, change in the stiffness of the fill caused by the annulus contraction, or borehole cut-off mechanisms due to the presence of clay seams. In hypersaline environments characterized by high corrosion rates, salt precipitation, and gas exsolution, the permeability of the open section of the borehole is expected to decrease by several orders of magnitude during the regulatory period. The k_{eff} for the entire borehole is unlikely to exceed approximately 10^{-14} m², even after the complete degradation of borehole plugs to amorphous silica.

Topic 6: Question on the initial degraded borehole permeability and effects of Closure Rates on PA

Regarding the initial degraded borehole permeability, the Agency considers the following conceptual assumptions in the Thompson model (not the PA simplification of that model) that were apparently accepted by Gjerapic et al. (2023) as defining the circumstances under which the upper bound permeability of the initial loose, uncompacted fill material should be determined.

a) *During the first 200 years after borehole drilling/abandonment and at depths below 300 to 350 m, pitting corrosion of the borehole casing occurs but the casing retains enough strength after 200 years to resist creep closure and maintain an open borehole for another 1,000 years that is filled with degradation debris falling from above.*

b) *During the first 200 years after borehole drilling/abandonment and at depths above 300 to 350 m, general corrosion begins and by 200 years the borehole casing and grout have completely degraded from general corrosion and the debris from expanding degradation products as well as geologic materials sloughed from above have completely filled the borehole from the Bell Canyon plug (or the lower Salado plug, whichever is uppermost) to above the Culebra member of the Rustler Formation.*

c) *The degradation debris filling the borehole at 200 years is a loose, uncompacted material for which a revised upper bound permeability is being proposed. Although this material is later*

subject to compaction from salt creep, this subsequent compaction does not affect its initial permeability.

Based on information provided by Gjerapic et al. (2023), EPA has identified several candidates for the upper bound, initial permeability of the loose, uncompacted borehole degradation debris envisioned in the Thompson model. These are summarized in Table 2 below.

Table 2. Summary List of Candidates for the Upper Bound Permeability of Degraded Borehole Fill and EPA Evaluation

Candidate Permeability	***Discussion***
10^{-10} m^2	*Initial permeability used by Gjerapic et al. (2023, p. 13) in calculating creep closure with upgraded Reedlunn et al. (2022) model; may be related to permeability of uncorroded iron PRB granules.*
10^{-11} m^2	*Upper bound permeability proposed by Thompson et al. (1996, p. 20) for a mixture of completely degraded grout, corroded casing, and sloughed geologic materials; this conceptual model was accepted by EPA.*
10^{-13} m^2	*Upper bound permeability cited by Gjerapic et al. (2023) and reported by Curtice and Mallow (1979) for samples of hydrothermal cement cured more than 14 days; EPA questions relevance to long-term degradation at WIPP.*
10^{-14} m^2	*Upper bound permeability proposed by Gjerapic et al. (2023, p. 8) for degraded borehole fill debris dominated by cement materials with limited confinement; primarily based on particle size distribution for a silty material (such as cement powders) and Hazen's equation correlating grain size distribution with permeability; EPA questions conceptual basis and uncertainty associated with this value.*

Note: Studies already considered by Thompson et al. (1996) were not included in this table.

RPPCR6-Bhperm-20: uncertainty regarding borehole debris fully consolidating to 10^{-15} m^2 permeability at repository depth

Please provide an assessment, based on an integrated conceptual model, of the uncertainty in the conclusion on page 15 that at the repository depth of about 650 m, the borehole debris is expected to fully consolidate under salt creep to a permeability on the order of 10^{-15} m^2, but under limited confinement would achieve the proposed maximum permeability of 10^{-14} m^2. Please address in this assessment the combined uncertainty resulting from the assumption of an initial degradation debris permeability of 10^{-10} m^2, uncertainty in the Reedlunn et al. (2022) creep model, uncertainty resulting from the creep model assumption that compressive strength of the degradation debris and pitted casing can be ignored, and uncertainty in the Kozeny-Carman model and its application to permeability reduction.

DOE Response

There is high confidence that the permeability of the debris-filled borehole will not exceed 10^{-14} m^2. The estimated 10^{-14} m^2 value should be viewed as a tail-end of the probability distribution for the upper bound borehole permeability because of the conservatism in the underlying assumptions including (but not limited to):

1. Continuous increase in the material confinement and deformation rates predicted from the rock salt creep model (see, for example, Reedlunn et al. 2022),

2. Predicted "effective" permeability values considering the long-term performance of cement plugs, available data on the cement grout and concrete degradation (see, for example, Pabalan et al. 2009, Matteo and Scherer 2012),

3. Industry practices for the design of structures in corrosive environments (see, for example, NPL 2020), and

4. WIPP-specific information on the performance of the installed cement plugs and conducted brine reservoir testing (see, for example, Bonen 1996, Christensen and Hunter 1980, Popielak et al. 1983).

Conceptually, it is believed that after 200 years initially open portions of the borehole will be filled with debris from degradation and slough from the borehole walls that will inhibit fluid flow. It has also been shown that this material will be subjected to significant confining stresses that will further restrict fluid flow. There are many sources of uncertainty in predicting the permeability of this degraded borehole. In setting an upper bound on the borehole permeability, we adopted a set of assumptions that lead to the least amount of flow restriction.

There is uncertainty in the debris filling the borehole and the permeability change due to that infilling. It is assumed the permeability of the borehole would decrease by at least one order of magnitude when filled with this debris. This is a conservative bound based on the assumption that debris consists of relatively large grains with a uniform size distribution. Specifically, the borehole debris filling is assigned a permeability value of 10^{-10} m^2 (without accounting for creep and changes due to long-term environmental exposures). The value of 10^{-10} m^2 is the highest permeability value reported for the manufactured porous iron-based material used in engineering practice (TAPRBI 2002) and a value reported in the literature on the degradation of cement grouts for fractured media under low confining pressures (Grandia et al. 2010).

Based on the work done by Reedlunn et al. (2022), the borehole infill is expected to be fully consolidated at a depth of 650 meters. A lower confining stress is conservatively assumed for the upper bound of possible borehole permeabilities. This assumption yields the maximum possible borehole permeability because it allows for borehole sections with relatively high permeability values (within parts of the borehole with an open annulus), while also accounting for the degradation scenario where the cement plug is completely degraded, ignoring the beneficial effects of plugging and cementation.

The compressive strength of degradation debris and pitted casing can be ignored due to the loose nature (low stiffness) of the degraded materials and the high stiffness and relatively large confining stresses (up to 20 MPa) of the surrounding rock mass. The expected variability (non-

uniformity) of degradation causes the section of the borehole to be completely degraded, with the debris falling into lower parts of the borehole.

The Kozeny-Carman equation has been shown to underestimate permeability reduction in the WIPP environment as the initial borehole permeability is reduced by 2 to 3 orders of magnitude or more (see, e.g., response to RPPCR6-Bhperm-14). It is, therefore, an appropriate prediction to use in bounding the maximum permeability for the borehole infill consisting of silty materials because it consistently overpredicts the "true" permeability value when calibrated for the pore size structure of materials with larger (initial) permeability (because it underpredicts the field-scale values of tortuosity and specific surface).

These assumptions result in a maximum borehole permeability of 10^{-14} m^2. This value represents the maximum permeability due to multiple highly conservative assumptions about borehole closure and sliding along clay seams (these effects are completely ignored), allowing for a scenario where the installed cement plugs are completely degraded (assuming a complete loss of cementation due to removal of calcium from the porous matrix), allowing for scenario where the large sections of the borehole remain under low confinement (i.e., disregarding beneficial effects of creep on the permeability reduction for upper parts of the Salado) and assuming the worst-case conditions in terms of the plug performance (it allows for the leaky interface between cement and steel or between cement and the surrounding rock without accounting for environmental conditions that are expected to result in the long-term plugging and sealing of preferential flow channels).

References RPPCR6-Bhperm-10-20

Allan, M.L. and Philippacopoulos, A.J. 1999. Properties and Performance of Cement-Based Grouts for Geothermal Heat Pump Applications - Final Report, FY 1999, Prepared for the Office of Geothermal Technologies, United States Department of Energy, under Contract No. DEAC02-98CH 10886, by Brookhaven National Laboratory, Materials and Chemical Sciences Division, Department of Applied Science, November.

American Society for Testing and Materials (ASTM International). 2020. Standard Practice for Classification of Soils for Engineering Purposes (Unified Soil Classification System). ASTM International. (ASTM D2487). DOI: 10.1520/D2487-17E01. www.astm.org.

American Society for Testing and Materials, ASTM International. 2017. Standard Test Methods for Particle-Size Distribution (Gradation) of Soils Using Sieve Analysis. ASTM International. (ASTM D6913). DOI: 10.1520/D6913-04R09E01. www.astm.org

American Society for Testing and Materials, ASTM International. 2021. Standard Test Method for Particle-Size Distribution (Gradation) of Fine-Grained Soils Using the Sedimentation (Hydrometer) Analysis. ASTM International. (ASTM D7928). DOI: 10.1520/D7928-21E01. www.astm.org.

Antonio, J.R.D. and Romero, J.T., 2020. Well Plugging Handbook. New Mexico Office of the State Engineer, accessed on September 15, 2024. https://www.ose.nm.gov/Statewide/Guidelines/2020%20Pluggінghandbook%20page%20format.pdf

Backe, K.R., Lile, O.B., Lyomov, S.K., Elvebakk, H. and Skalle, P. 1999. Characterizing Curing-Cement Slurries by Permeability, Tensile Strength and Shrinkage, SPE Drilling & Completion, Vol. 14, No. 3, pp. 162-167.

Bardet, J.P. 1997. Experimental Soil Mechanics. Prentice Hall, Inc. New Jersey.

Bear, J. 1972. Dynamics of Fluids in Porous Media. American Elsevier Publishing Company Inc. New York. Re-print by Dover Books Inc. 1988.

Bonen, D., 1996, "Petrographic Analyses of Concrete and Grout Recovered from the WIPP," The Technological Institute, Northwestern University, Interim Report, January 15, 1996, 9pp.

Breedon Group (Breedon). 2024. Portland Plus Cement - The UK's Premium Cement – Technical Data Sheet, https://www.breedongroup.com/, downloaded on November 5, 2024.

British Standards Institution (BSI), Maritime Structures, Parts 1 and 2, BS 6349: Part 1 and 2:1984, 1988, BSI Standards, London, England, 1988.

Carrier, W D. 2003. Goodbye, Hazen; Hello, Kozeny-Carman. ASCE Journal of Geotechnical and Geoenvironmental Engineering, November, pp. 1054–1056.

Christensen, C.L. and Hunter, T.O. 1980. "The Bell Canyon Test and Results'' SAND80-2414C. Sandia National Laboratories, Albuquerque NM. https://www.osti.gov/servlets/purl/7177549.

Christensen, B.J., Mason, T.O. and Jennings, H.M. 1996. Comparison of Measured and Calculated Permeabilities for Hardened Cement Pastes. Cement and Concrete Research, Vol. 26, No. 9, pp. 1325-1334. Elsevier Science Ltd.

Clennell, M.B. 1997. Tortuosity: a guide through the maze, from Developments in Petrophysics, Lowell, M.A. & Harvey, P.K. (eds), Geological Society Special Publication No. 122, pp. 299-344.

Corey, A. 1977. Mechanics of Immiscible Fluids in Porous Media. Water Resources Publications, pp. 272. ISBN -13: 978-0-918334-83-1

Cowie, K. 2009. Steel Corrosion Rates in Water and Soil. Steel construction New Zealand, Inc., Ref. No. CRG1006. https://scnz.org/wp-content/uploads/2020/12/CTG1006.pdf.

Curtice, D.K and Mallow W.A. 1979. Hydrothermal Cements for Use in the Completion of Geothermal Wells, report prepared by the Southwest Research Institute, BNL Contract No. 427964-S, BNL-51183, UC-66d - Geothermal Utilization Technology- TID-4500 for the Geothermal Materials Group, Department of Energy and Environment, Brookhaven National Laboratory Associated Universities Inc., under contract No. DE-AC02-76CH00016 with the United States Department of Energy

Di Emidio, G. Verástegui Flores, R.D. and Van Impe, W.F. 2009. Crushability of Granular Materials at High Stress Levels. Proc. of the 17th International Conference on Soil Mechanics and Geotechnical Engineering, M. Hamza et al. (Eds). October 5-9, 2009, Alexandria, Egypt. pp. 127-130. doi:10.3233/978-1-60750-031-5-127.

Diaz-Mateus, M.A., Machuca, L.L., Farhat, H. and Salgar-Chaparro S.J. 2024. Synergistic corrosion effects of magnetite and microorganisms: microbial community dependency. Appl Microbiology and Biotechnology, 2024 Mar 5;108(1):253. doi: 10.1007/s00253-024-13086-6. PMID: 38441693; PMCID: PMC10914896.

DOE (U.S. Department of Energy) 1996. Title 40 CFR Part 191, Compliance Certification Application for the Waste Isolation Pilot Plant. DOE/CAO 1996-2184. U.S. Department of Energy, Carlsbad New Mexico. October.

DOE (U.S. Department of Energy) 2018. Delaware Basin Monitoring Annual Report, September 2018. DOE/WIPP-18-2308, Rev. 1. Carlsbad Field Office, Carlsbad, New Mexico. September.

DOE (U.S. Department of Energy) 2022. Delaware Basin Monitoring Annual Report, September 2022. DOE/WIPP-22-2308, Rev. 0. Carlsbad Field Office, Carlsbad, New Mexico. December.

DOE (U.S. Department of Energy) 2024. Planned Change Request for the Use of Replacement Panels 11 and 12. CBFO:ERCD:MG:SV:24-0168. Carlsbad Field Office, Carlsbad, New Mexico. March.

Eggleston, J. and Rojstaczer, S. 2001. The Value of Grain-Size Hydraulic Conductivity Estimates: Comparison with High Resolution In-Situ Field Hydraulic Conductivity. Geophysical Research Letters, Vol. 28, No. 22, pp. 4255-4258, November 15, 2001.

EPA (U.S. Environmental Protection Agency) 1998a. Technical Support Document for Section 194.23, Sensitivity Analysis Report. Docket No. A-93-02, V-B-13. Office of Radiation and Indoor Air, Washington DC. May.

EPA (U.S. Environmental Protection Agency) 1998b. Technical Support Document for Section 194.23, Parameter Justification Report. Docket No. A-93-02, V-B-14. Office of Radiation and Indoor Air, Washington DC. May.

Ferraris, C.F., Hackley, V. and Avilés, A.I. 2004. Measurement of Particle Size Distribution in Portland Cement Powder: Analysis of ASTM Round Robin Studies, in Cement, Concrete and Aggregates, Vol. 26, No. 2., https://tsapps.nist.gov/publication/get_pdf.cfm?pub_id=860497.

Freeze, R. Allan, and Cherry, John A. 1979. Groundwater. Prentice Hall, Englewood Cliffs, NJ.

Gjerapic, G., Bean, J.L., Matteo, E.N. and Gross, M.B. 2023. Analyses to Bound the Permeability of Degraded Fill Materials in Intrusion Boreholes for WIPP Performance Assessment. ERMS 579102. Carlsbad, NM: Salado Isolation Mining Contractors, LLC.

Grandia, F. Galindez, J.M., Arcos, D., Amphos, J. M. 2010. Quantitative modeling of the degradation processes of cement grout – Project CEMMOD – Technical Report TR-10-25. Swedish Nuclear Fuel and Waste Management Company. https://www.skb.com/publication/2042105/TR-10-25.pdf

Hattamleh, O.H., Al-Deeky, H.H. and Akhtar, M., N. 2013. The Consequence of Particle Crushing in Engineering Properties of Granular Materials. *International Journal of Geosciences*, Vol. 4 No. 7, pp. 1055-1060. doi: 10.4236/ijg.2013.47099.

Hazen, A. 1892, Physical Properties of Sands and Gravels With Reference to Their Use Infiltration, Massachusetts State Board of Health, Boston, Mass. (as referenced in Wang et al. 2017).

He, Y., Cai, G., Gao, L. and He, H. 2022. Effects of Particle Size and Constraint Conditions on Single Particle Strength of Carbonate Sand, Sensors. Vol. 22, No. 765. https://doi.org/10.3390/s22030765.

International Organization for Standardization – Corrosion of metals and alloys (ISO 9223), ISO9223:2012, https://www.iso.org/standard/53499.html.

Johnson, R. and Tratnyek, P. 2008. Remediation of Explosives in Groundwater Using a Zero-Valent Iron Permeable Reactive Barrier, Department of Defense Environmental Security Technology Certification Program. ESTCP Project ER-0223. Final Report, May 2008.

Kulhawy, F.H. and Mayne, P.W. 1990. Manual on Estimating Soil Properties for Foundation Design, Report EL-9800 to Electric Power Research Institute, Cornell University, Ithaca, New York.

Lanfrey, P.-Y., Z.V. Kuzeljevic, and M.P. Dudukovic. 2010. Tortuosity model for fixed beds randomly packed with identical particles. Chem. Eng. Sci. 65:1891– 1896. doi:10.1016/j.ces.2009.11.011

Lade, P.V., Yamamuro, J.A. and Bopp, P.A. 1996. Significance of Particle Crushing in Granular Materials. J. Geotech. Engrg., 1996, 122(4): 309-316.

Loudon, A. G. 1952. ‘‘The computation of permeability from simple soil tests.’’ Geotechnique, Vol. 3, No. 4. pp. 165–183. https://doi.org/10.1680/geot.1952.3.4.165

Marín, R.R.R, Babick, F., Lindner, G.G., Wiemann, M. and Stintz, M. 2018. Effects of Sample Preparation on Particle Size Distributions of Different Types of Silica in Suspensions, in Nanomaterials (Basel). Published on Jun 21, 2018; 8(7):454. doi: 10.3390/nano8070454. PMID: 29933581; PMCID: PMC6070795.

Matteo, E.N. and Scherer, G.W. 2012. Experimental study of the diffusion-controlled acid degradation of Class H Portland cement, International Journal of Greenhouse Gas Control, Vol 7, pp. 181-191, ISSN 1750-5836, DOI: 10.1016/j.ijggc.2011.07.012

Mentellato, S., Palacios, M. and Flatt, R.J. 2015. Reliable specific surface area measurements on anhydrous cements, Cement and Concrete Research, Vol. 67. pp. 286-291. http://dx.doi.org/10.1016/j.cemconres.2014.10.009

Mills, R. Van A. 1926. Corrosion in Oil and Gas Wells – Its Causes and Prevention, Transactions of the AIME, Society of Petroleum Engineering (SPE), SPE -926589-G, pp. 589-597. (https://doi.org/10.2118/926589-G).

Moraci, N., Ielo, D., Bilardi, Sand Calabro, P.S. 2016. Modelling Long Term Hydraulic Conductivity Behavior of Zero Valent Iron Column Tests for PRB Design. Canadian Geotechnical Journal, Vol. 53, No. 6. June 2016.

National Physical Laboratory (NPL), 2020, Guides to Good Practice in Corrosion Control No. 12 – Atmospheric Corrosion. Report prepared by Prof. Stuard Lyon, the University of Manchester on behalf of the National Corrosion Service., United Kingdom.

Pabalan, R.T., Glasser, F.P., Pickett, D.A., Walter, G.R., Biswas, S., Juckett, M.R., Sabido, L.M. and Myers, J.L. 2009. Review of Literature and Assessment of Factors Relevant to Performance of Grouted Systems for Radioactive Waste Disposal. Report prepared for U.S. Nuclear Regulatory Commission under contract No. NRC-02-07-006. Report No. CNWRA 2009-001.

Pap, M. and Mahler, A. 2021. Prediction of permeability coefficient for Quaternary Sediments of Drava River using different empirical correlations. 6th International Conference on Geotechnical and Geophysical Site Characterization, Budapest, Hungary, September 26-29, 2021. https://www.issmge.org/uploads/publications/25/111/ISC2020-534.pdf

Paine, K.A. 2019. Physicochemical and Mechanical Properties of Portland Cements, in Lea's Chemistry of Cement and Concrete (Fifth Edition), Peter C. Hewlett, Martin Liska editors, Butterworth-Heinemann, pp. 285-339, ISBN 9780081007730, https://doi.org/10.1016/B978-0-08-100773-0.00007-1.

Popielak, R.S., Beauheim, R.L., Black, S.B., Coons, W.E., Ellingston, C.T., and R.L. Olsen. 1983. Brine Reservoirs in the Castile Formation, Waste Isolation Pilot Plant (WIPP), Southeastern New Mexico. Project TME-3153. Westinghouse Electric Corporation, Carlsbad, N.M.

Popp, T., Minkley, W., Fillinger, E. and Boettge, V. 2018. Closure of the Teutschenthal backfill mine – About the challenge to elaborate a geomechanical safety concept in salt formations, Proc. of the 9th Conference on the Mechanical Behavior of Salt (SaltMech IX), Hannover, Germany, 12-14 September 2018.

Reedlunn, B., Argilello, J.G., and Hansen F.D. 2022. A reinvestigation into Munson's model for room closure in bedded rock salt, International Journal of Rock Mechanics and Mining Sciences, Volume 151, ISSN 1365-1609.

Roselle, G. T. 2013. Determination of Corrosion Rates from Iron/Lead Corrosion Experiments to be used for Gas Generation Calculations (Revision 1). Analysis Report, January 23, 2013. Sandia National Laboratories, Carlsbad, NM. ERMS 559077

Saiyouri, N., Alaiwa, A.A. and Hicker, P.Y. 2011. Permeability and porosity improvement of grouted sand, European Journal of Environmental and Civil Engineering, Taylor & Francis, Vol. 15, No. 3, pp. 77-97.

Stormont, J.C., Fernandez, S.G. Taha, M.R and Matteo, E.N. 2018. Gas flow through cement casing microannuli under varying stress conditions, Geomechanics for Energy and Environment, Vol 13, pp. 1-13, DOI: 10.1016/j.gete.2017.12.001

Subramanian, K.H. 2008. Life Estimation of High Level Waste Tank Steel for F-Tank Farm Closure Performance Assessment, Rev. 2. Savannah River National Laboratory Materials Science and Technology Directorate. Washington Savannah River Site Aiken SC 29808. https://www.nrc.gov/docs/ML1112/ML111240593.pdf

TAPRBI (Tri-Agency Permeable Reactive Barrier Initiative). 2002. United States Department of Defense, U.S. Department of Energy and U.S. Environmental Protection Agency and Interstate Technology and Regulatory Council. Report prepared for Federal Remediation Technologies Roundtable (FRTR). https://www.epa.gov/sites/default/files/2015-04/documents/2-prbperformance_web.pdf

Terzaghi, K. and Peck, R.B. 1967. Soil Mechanics in Engineering Practice, 2nd Edition, John Wiley & Sons, New York, pp. 729.

Thompson, T.W., W.E. Coons, J. L. Krumhansl, and F.D. Hansen 1996. Inadvertent Intrusion Borehole Permeability. Title 40 CFR Part 191, Compliance Certification Application for the Waste Isolation Pilot Plant. Appendix MASS, Attachment 16-3. U.S. Department of Energy, Carlsbad New Mexico. July.

USBR (U.S. Bureau of Reclamation). 1987. *Design of Small Dams.* Third Edition, U.S. Bureau of Reclamation, Denver, Colorado.

Vipulanandan, C. and Mohammed, A. 2020. Effect of drilling mud bentonite contents on the fluid loss and filter cake formation on a field clay soil formation compared to the API fluid loss method and characterized using Vipulanandan models, Journal of Petroleum Science and Engineering, Vol. 189, ISSN 0920-4105, https://doi.org/10.1016/j.petrol.2020.107029.

Wagner, S. and Hillesheim, M. 2009. Sandia National Laboratory Compliance Monitoring Parameter Assessment for 2009. Report No. WIPP:1.3.1:CO:QA-L:pkg 510062 prepared for the United States Department of Energy, November 2009.

Wang, J.-P., Francois, B., and Lambert, P. 2017. Equations for hydraulic conductivity estimation from particle size distribution: A dimensional analysis, Water Resour. Res., 53, 8127– 8134, doi:10.1002/2017WR020888.

Yan, F., Tuller, M., de Jonge, L.W., Moldrup, P. and Arthur, E. 2023. Specific surface area of soils with different clay mineralogy can be estimated from a single hygroscopic water content, Geoderma, Vol. 438, ISSN 0016-7061, https://doi.org/10.1016/j.geoderma.2023.116614.

Yurtdas, I., Xie, S., Secq, J., Burlion, N., Shao, J.F., Rodot, F. 2010. Influence of chemical degradation on the mechanical behaviour-permeability coupling of an oil well cement paste under temperature. Proceedings of Fracture Mechanics of Concrete and Concrete Structures – Assessment, Durability, Monitoring and Retrofitting of Concrete Structures, B.H. Oh et al. (eds), 2010 Korea Concrete Institute, Seoul, ISBN 978-89-5708-181-5, https://framcos.org/FraMCoS-7/08-14.pdf.

Yurtdas, I. Xie, S.Y., Burlion, N., Shao, J.F., Saint-Marc, J. and Garnier, A. 2011. Deformation and Permeability Evolution of Petroleum Cement Paste Subjected to Chemical Degradation Under Temperature. Transp. Porous Med. Vol. 86. pp. 719-736, https://doi.org/10.1007/s11242-010-9648-y

Zeitler, T.R. 2018a. Cumulative Distribution for STEEL:CORRMCO2 for the CRA-2019 PA. Carlsbad, NM: Sandia National Laboratories. December 12, 2018, ERMS 570869

Zeitler, T.R. 2018b. Bounding Calculation of the Cumulative Distribution for STEEL:HUMCORR. Carlsbad, NM: Sandia National Laboratories. April 30, 3028, ERMS 569807

Enclosure 2

Department of Energy Response 8

Status Report of DOE Responses To EPA Questions on the RPPCR

Status Report of DOE Responses to EPA questions on the RPPCR			
EPA Comment Number	**EPA Request Description**	**EPA Request Letter Date**	**DOE Response**
RPPCR1-References-1	Document Request	April 17, 2024	Response 1
RPPCR2-General-1	Dimensions of replaced area and new panels	April 24, 2024	Response 1
RPPCR1-PROPMIC-1	Pu(III) PROPMIC and CAPMIC values	April 17, 2024	Response 2
RPPCR2-12 PanelAnalyses	12 Panel Analyses	April 24, 2024	Response 2
RPPCR3-Closure-1	Closure of rooms with new design	May 10, 2024	Response 2
RPPCR1-Inventory-1	Waste Characteristics	April 17, 2024	Response 2
RPPCR1-DTAT0.FM6-1	Documentation for Hydromagnesite5424 Solubility	April 17, 2024	Response 2
RPPCR2-DATA0.FM6-4	Omitted Pitzer interaction parameters	April 24, 2024	Response 2
RPPCR-Inventory-2	Breakdown of Emplaced and Temporary Storage CH and RH Waste Volumes by Waste Generator Site	April 17, 2024	Response 3
RPPCR2-DATA0.FM6-1: a-c	$Am(OH)_3(am)$ verification calculations at low ionic strength	April 24, 2024	Response 3
RPPCR2-DATA0.FM6-2: a-c	$Am(OH)_3(am)$ verification calculations at high ionic strength	April 24, 2024	Response 3
RPPCR2-DATA0.FM6-3	$AmOHCO_3(c)$ verification calculations	April 24, 2024	Response 3
RPPCR1-DATA0.FM6-2: a-c	XRD Examination of Post-Test Solids	April 17, 2024	Response 3
RPPCR1-DATA0.FM6-3: a-b	WIPP Test Plans Cited in DATA0.FM6 Documentation	April 17, 2024	Response 3
RPPCR1-DATA0.FM6-4	$FeEDTA^{2-}$ Stability Constant	April 17, 2024	Response 3
RPPCR1-DATA0.FM6-5	$FeCitrate^{-}$ Stability Constant	April 17, 2024	Response 3
RPPCR1-DATA0.FM6-9	Cerussite Solubility	April 17, 2024	Response 3

Status Report of DOE Responses to EPA questions on the RPPCR			
EPA Comment Number	**EPA Request Description**	**EPA Request Letter Date**	**DOE Response**
RPPCR1-OXCUTOFF-1: a-b	Sensitivity study using OXCUTOFF parameter	April 17, 2024	Response 4
RPPCR4-Corrosion-1	Steel Packaging and Waste Iron-Based Metals/Alloys Surface Area Recalculation	June 27, 2024	Response 4
RPPCR4-Corrosion-2	Recalculation of Ds	June 27, 2024	Response 4
RPPCR1-DATA0.FM6-6	Cotunnite Solubility	April 17, 2024	Response 4
RPPCR1-DATA0.FM6-8: a-b	Hydrocerussite Solubility	April 17, 2024	Response 4
RPPCR3-BRAGFLO-1	Follow up on BRAGFLO convergence	May 10, 2024	Response 4
RPPCR1-DBMAR-1: a-d	Questions related to the DBMAR	April 17, 2024	Response 5
RPPCR5-12PanelAnalyses-1	N/A	August 12, 2024	Response 5
RPPCR5-12PanelAnalyses-2	N/A	August 12, 2024	Response 5
RPPCR5-12PanelAnalyses-3	N/A	August 12, 2024	Response 5
RPPCR5-12PanelAnalyses-4	N/A	August 12, 2024	Response 5
RPPCR5-12PanelAnalyses-5	N/A	August 12, 2024	Response 5
RPPCR5-12PanelAnalyses-6	Effects of 12-Panel vs. 19-Panel Minimum Brine Volumes on Actinide Solubilities and Repository Releases	August 12, 2024	Response 5
RPPCR1-EM-1: a-e	Questions about the EM survey	April 17, 2024	Response 6
RPPCR3-Mineralogy-1	Detailed mineralogy of new panels	May 10, 2024	Response 6

Status Report of DOE Responses to EPA questions on the RPPCR			
EPA Comment Number	**EPA Request Description**	**EPA Request Letter Date**	**DOE Response**
RPPCR7-BrineRes-5	further description and explanation of revised geometric representation of Castile brine reservoir in BRAGFLO	September 27, 2024	Response 6
RPPCR7-BrineRes-6	difference in BRAGFLO grid representation between Docherty (2023) and RPPCR PA (DOE, 2024)	September 27, 2024	Response 6
RPPCR7-BrineRes-1	acceptance of calibration curves after ~400 hours	September 27, 2024	Response 7
RPPCR7-BrineRes-2	causes of field pressure peak and decline in long-term shut-in test	September 27, 2024	Response 7
RPPCR7-BrineRes-3	uncertainties and the 162 psig as final reservoir equilibrium pressure	September 27, 2024	Response 7
RPPCR7-BrineRes-4	basis for estimate of maximum brine reservoir pore volume	September 27, 2024	Response 7
RPPCR1-DATA0.FM6-7	Lead-Carbonate Aqueous Speciation	April 17, 2024	Response 7
RPPCR6-Bhperm-1:	PRB granules as surrogates for corroded borehole casing Please provide justification that include relevant experiments, data, and literature citations	September 5, 2024	Response 8
RPPCR6-Bhperm-2:	discrepancy in upper bound permeability for degraded steel casing	September 5, 2024	Response 8
RPPCR6-Bhperm-3:	PRB column test conditions	September 5, 2024	Response 8
RPPCR6-Bhperm-4:	scatter and uncertainty in experimental results of Moraci et al. (2016)	September 5, 2024	Response 8
RPPCR6-Bhperm-5:	relevance of Moraci et al. column tests to WIPP conditions	September 5, 2024	Response 8
RPPCR6-Bhperm-6:	PRB corrosion test results and Thompson model	September 5, 2024	Response 8
RPPCR6-Bhperm-7:	PRB degredation and incomplete degredation	September 5, 2024	Response 8
RPPCR6-Bhperm-8:	concrete grout degrading to silt-like powders	September 5, 2024	Response 8

Status Report of DOE Responses to EPA questions on the RPPCR			
EPA Comment Number	**EPA Request Description**	**EPA Request Letter Date**	**DOE Response**
RPPCR6-Bhperm-9:	uncertainty in predicted permeability of Hazen equation	September 5, 2024	Response 8
RPPCR6-Bhperm-10:	coarser grained materials in degredation debris and permeability	September 5, 2024	Response 8
RPPCR6-Bhperm-11:	relevance of microannuli permeability laboratory results	September 5, 2024	Response 8
RPPCR6-Bhperm-12:	relevance of continuity calculation	September 5, 2024	Response 8
RPPCR6-Bhperm-13:	description and significance of maximum creep volume loss	September 5, 2024	Response 8
RPPCR6-Bhperm-14:	uncertainty associated with predicted permeability using Kozeny-Carman relationship	September 5, 2024	Response 8
RPPCR6-Bhperm-15:	explanation and timeline of conceptual model for surface hole, upper salt section, and lower salt section	September 5, 2024	Response 8
RPPCR6-Bhperm-16:	sample calculations using Kozeny-Carman method	September 5, 2024	Response 8
RPPCR6-Bhperm-17:	applicability of Kozeny-Carman model for fine-grained borehole degredation debris	September 5, 2024	Response 8
RPPCR6-Bhperm-18:	initial permeability of degraded borehole debris used in creep closure analysis	September 5, 2024	Response 8
RPPCR6-Bhperm-19:	effect of backpressure buildup on reductions in permeability in updated modeling	September 5, 2024	Response 8
RPPCR6-Bhperm-20:	uncertainty regarding borehole debris fully consolidating to 10^{-15} m^2 permeability at repository depth	September 5, 2024	Response 8
End of Status Report			